Lower Hybrid current drive in high aspect ratio tokamaks

Y Peysson, D Mazon, J-F Artaud, A Ekedahl, L Delpech, J Hillairet, T Hoang, X L Zou, X y Bai, Y P Zhang, et al.

Lower Hybrid current drive in high aspect ratio tokamaks

[1]**Y Peysson, D Mazon, J-F Artaud, A Ekedahl, L Delpech, J Hillairet, T Hoang, X L Zou and WEST Team***

[2]**X Y Bai, Y P Zhang and HL-2A Team**

[3]**K Krol, J Bielecki, A Jardin, M Scholz, D Dworak**

[4]**J Decker**

[1]CEA, IRFM, F-13108, Saint-Paul-lez-Durance, France
[2]Southwestern Institute of Physics (SWIP), No. 5, Huangjing road, Shuangliu, Chengdu 610225, China
[3]Institute of Nuclear Physics Polish Academy of Sciences (IFJ PAN), PL-31-342, Krakow, Poland.
[4]Ecole Polytechnique Fédérale de Lausanne (EPFL), Centre de Recherches en Physique des Plasmas (CRPP), CH-1015 Lausanne, Switzerland
*http://west.cea.fr/WESTteam

E-mail: yves.peysson@cea.fr

Abstract. A multi-machine study has been carried out to investigate the impact of a strongly bounded wave propagation domain on the Lower Hybrid current drive, a condition which occurs principally in high aspect ratio tokamaks. In this regime, the condition of kinetic resonance can be far above the upper boundary of the propagation domain, and may not be achieved by the usual toroidal upshift. Therefore no tail of fast electrons can be pulled out from the thermal bulk. Nevertheless, while tokamak plasmas are in principle almost transparent to the wave in this regime so-called "unbridgeable spectral gap", full current drive is well achieved for the two tokamaks considered in this study, TRIAM-1M [H. Zushi, et al., Nucl. Fusion 43 (2003) 1600] and WEST [C. Bourdelle, et al., Nucl. Fusion 55 (2015) 063017], both characterized by a very large aspect ratio $R/a > 5.5$. The case of the high aspect ratio tokamak HL-2A [Y. Liu et al. Nucl. Fusion 45 (2005) S239] for which the wave propagation domain has also an upper boundary, but close to the resonance condition, is considered by comparison. First principles modeling of the rf-driven current and the fast electron bremsstrahlung using the ALOHA/C3PO/LUKE/R5-X2 chain of codes shows unambiguously that the spectral gap must be already filled at the separatrix in order to reproduce quantitatively observations and some important parametric dependencies. This result is an important milestone in the physics understanding of the Lower Hybrid current drive, highlighting the existence of a powerful and likely universal alternative mechanism to bridge the spectral gap, that is not related to toroidal magnetic refraction. With an initially broad power spectrum, lobes with low parallel refractive indexes that carry most of the plasma current can be absorbed in almost single pass, restoring the full validity of the ray-tracing approximation for describing the propagation of the Lower Hybrid wave in cold plasmas.

Keywords: 52.50.Sw, 52.55.Wq

1. Introduction

The Lower Hybrid (LH) wave has received a considerable interest during the last decades owing to its attractive property of damping efficiently at high parallel (to B) phase velocities relative to the electron thermal speed [1, 2]. As expected from theory, a high figure of merit of the current drive efficiency has been achieved, while the control of the current density profile has been successfully demonstrated in several machines [3–7]. However, in almost all experimental conditions, the parallel phase velocity of the LH wave $v_{\phi\|0}$ at launch is much higher than the thermal velocity v_{Te} of the bulk electrons, raising the question of the damping mechanism, known as the "spectral gap" problem. Indeed, strong linear wave damping on a Maxwellian distribution requires $v_{\phi\|}$ to reach $v_{\phi\|L} \sim 3.5 \times v_{Te}$ approximately, which is equivalent at fixed LH frequency to the condition $N_\| \simeq N_{\|L}$ where $N_\| = c/v_{\phi\|}$ is the parallel (to B) refractive index of the LH wave and $N_{\|L} = c/v_{\phi\|L} \simeq 6.5/\sqrt{T_e\,[keV]}$. Here, T_e is the local electron temperature in units of keV and c the speed of light [8, 9] . It is assumed that LH power density in the plasma is low enough for neglecting parametric instabilities which may contribute to slightly shift the launched LH frequency inside the plasma.

Many mechanisms have been suggested to explain how a tail of supra-thermal electrons can be pulled out from the thermal distribution. Most of them consider a progressive modification of the LH power spectrum from the antenna to the damping region such that the resonant Landau absorption can take place continuously from the edge to the core of the plasma. Since $N_\|$ varies during its propagation in the plasma as a consequence of the poloidal non-uniformity of the magnetic field, this mechanism has been considered as universal for toroidal magnetic configurations like tokamaks, to fill the spectral gap [10, 11]. Consequently, combined ray-tracing (RT) and Fokker-Planck (FP) calculations have almost become a standard for solving the spectral gap problem and simulate LH current drive experiments, even if full-wave calculations have been successfully performed more recently, removing the well-known limitations of the WKB approximations at some specific locations of the ray trajectories [1, 2, 12–14]. Nevertheless, advanced modeling techniques have never been conclusive, and despite their intrinsic limitations, RTFP calculations remain widely used for LH current drive calculations.

When plasma conditions are such that the spectral gap is rather narrow for a given value of $N_{\|0} = c/v_{\phi\|0}$, i.e. when $\delta_{N_{\|0}} = \left(N_{\|L}^{\min} - N_{\|0}\right)/N_{\|0} < 1$, experimental observations can be reproduced quantitatively by RTFP calculations considering only toroidal refraction, in particular Fast Electron Bremsstrahlung (FEB) line-integrated profiles in the Hard X-Ray (HXR) range of photon energies, as shown for plasmas in Tore Supra tokamak [6]. Here, $N_{\|L}^{\min}$ is the minimal value of $N_{\|L}$ in the plasma. However, when $\delta_{N_{\|0}} \gg 1$, which corresponds to the criterion of a large spectral gap, simulations exhibit almost systematically a poor agreement against experimental observations and a large sensitivity to smallest changes in the calculation parameters (launching conditions, toroidal MHD equilibrium, ...), a signature of the Hamiltonian chaos in the ray dynamics resulting from toroidicity [15–18]. Indeed, in this regime, power absorption of the LH wave in the plasma is usually very weak, taking place after an integration time exceeding largely the maximal Liapunov exponent, which characterizes the rate of separation of infinitesimally close ray trajectories [19]. Consequently, RT has in principle lost its physical meaning, since no wavefront can be defined, and the memory of initial conditions is lost. Nevertheless, full absorption can take place when the ray lengths are long enough in this regime, because in most LH current drive experiments, the wave propagation domain is not bounded towards high $N_\|$values even if $\delta_{N_{\|0}} \gg 1$. However, experimental observations never bear the signature of a strong sensitivity to plasma parameters,

typical of a stochastic regime, and moreover, FEB dependencies with some wave characteristics at launch indicate unambiguously that memory is not fully lost from the antenna to the place where it is absorbed [3, 18]. These facts suggest that other efficient physical absorption mechanisms still exist for all values of $\delta_{N_{\parallel 0}}$, which results in valid RT calculations even when the spectral gap is large.

In this context, it has been suggested that the LH power spectrum could be already broad at the separatrix, restoring consequently an almost single-pass absorption in the core plasma consistent with the conditions of validity of the RT, whatever the width of the spectral gap [20]. The combination of toroidal refraction with a broad power spectrum leads to a smooth transition from $\delta_{N_{\parallel 0}} < 1$ to $\delta_{N_{\parallel 0}} \gg 1$. The so-called "tail spectral model (TSM)" which describes this broadening has been studied first for high density and low temperature discharges in the Tore Supra tokamak, and a good agreement between experimental FEB observations and simulations has been found if more than 50 % of the power carried by the main lobe of the excited power spectrum is transferred to the tail, described as a succession of secondary lobes, up to $N_{\parallel L}^{\min}$ [18]. Interestingly, the level of agreement is rather weakly sensitive to the fraction of power in the tail as far as it exceeds 50 %. With the TSM that can be interpreted as a fluctuating power spectrum on a time scale shorter than fast electron collisional slowing-down, the FEB profile at high photon energies can be well reproduced by RTFP simulations but also variations of the FEB characteristics with $N_{\parallel 0}$. This successful achievement has been extended to the modeling of the LH current drive in elongated diverted plasmas for ALCATOR C-Mod and EAST tokamaks, using the same simulation parameters for the TSM, in particular the fraction of the LH power transferred from the main lobe to the tail [2, 19]. A possible explanation of this spectral broadening in the scrape-off layer may be fast longitudinal plasma density fluctuations in front of the antenna that diffract the LH wave [21]. Indeed, rotation of the perpendicular component of the wave vector, the only degree of freedom in the LH propagation, thanks to the interaction between the LH wave and possible low frequency edge density fluctuations described by electron drift waves cannot lead to a significant spectral broadening in $N_{\parallel}$, since locally, the magnetic field is an almost axis of symmetry [22]. Consequently, $N_{\parallel}$ is not evolving at the scale of the perturbation, being a constant of the ray motion. Recently, several experimental investigations of the spectral characteristics of the LH wave near the separatrix have been carried out [23, 24]. They will give certainly valuable details on the LH wave characteristics before entering the core plasma and contribute to improve the understanding of the overall LH wave dynamics.

If such encouraging results clearly pinpoint the potential importance of the plasma edge on the core LH physics, it turns out that studied discharges on which the TSM has been successfully tested are all characterized by an open spectral domain of propagation [25]. In this case, the upshift of $N_{\parallel}$ is not bounded in the core plasma, and the condition of resonance $N_{\parallel} = N_{\parallel L}$ may be always encountered if one or multiple physical mechanisms exist in the core plasma to broaden the power spectrum as the LH wave propagates. Conversely, if the spectral domain of propagation of the LH wave is strongly bounded by a KAM (Kolmogorov-Arnold-Moser) surface corresponding to an upper spectral limit $N_{\parallel KAM}$ with $N_{\parallel KAM} \ll N_{\parallel L}^{\min}$, the condition of resonance may never be achieved as far as $\delta_{N_{\parallel 0}} \gg 1$. In this regime, so-called "unbridgeable spectral gap", the core plasma is transparent to the wave, and it propagates indefinitely bouncing between boundaries of the domain, i.e. caustic and cut-off, as the LH wave do not propagate in vacuum. At each pass near the plasma edge where cuts-off occur, a small fraction of the power carried by the LH wave is transferred to the plasma by non-resonant collisional interaction, and this process takes place until full damping is achieved [26]. Consequently, since no tail of fast electrons can be pulled out from the thermal distribution function

in this regime, the LH wave is in principle unable to drive any toroidal current in the plasma. Such a regime can be easily achieved in large aspect ratio tokamak since toroidal mode coupling in the wave propagation is almost negligible, which makes this type of machine particularly interesting to investigate the spectral gap problem.

Despite this strong limitation which in principle fully forbid the absorption of the LH wave, full LH current drive has been successfully and reproducibly obtained in the small tokamak TRIAM-1M, characterized by a very large mean aspect ratio $\bar{\mathcal{A}}$ exceeding 7.5. In this case, whatever the operating plasma parameters, the extremely bounded propagation domain, as shown in Fig. 1, should prevent the formation of any fast electron tail, what is not shown experimentally [27]. Such a paradox has been identified and studied long time ago [28], and from full-wave calculations coupled with a FP code, it has been suggested that the LH power spectrum must be already broad at the separatrix, in order to drive the full toroidal current, as observed experimentally [20], which led later to develop the TSM for RT calculations [18].

In this paper, the fundamental role of the spectral broadening at the periphery of the plasma is investigated by studying full LH current drive in two tokamaks, TRIAM-1M [29] and WEST [30] for which the condition on unbridgeable spectral gap $\delta_{N_{\parallel 0}} \gg 1$ is well fulfilled. The case of the full LH current drive in the high aspect ratio tokamak HL-2A [31], for which the spectral gap is much smaller while the excited power spectrum has many lobes, is considered by comparison. In Sec. 2, the kinematics of the LH wave in a tokamak is first described and discussed, following the work designed to study impact of the poloidal field and plasma shape on LH wave propagation in the tokamak PBX-M [25]. An original criterion is derived to characterize plasmas for which the condition of an unbridgeable spectral gap exists. In Sec. 3, full current drive simulations are carried out using the well validated set of codes : Lower Hybrid antenna coupling ALOHA [32], 3-D ray-tracing C3PO [33], 3-D linearized relativistic bounce-averaged electron Fokker-Planck solver LUKE [34] and quantum relativistic bremsstrahlung code R5-X2 [35]. Finally, main results are summarized in Sec. 4, and conclusions on LH wave modeling in tokamaks are drawn. All simulation parameters are summarized in Tab. 1.

2. Kinematics of the LH wave

Using notations defined in Ref. [33], the range of $N_\parallel$ accessible to the excited LH wave may be determined locally by the cold dispersion relation $\mathcal{D}(\mathbf{k},\omega)=0$, which defines implicitly the function $k_\perp^2\left(k_\parallel\right)$ where

$$k_\parallel = \sigma_I \mathcal{P}\frac{m}{r}\cos\alpha + \sigma_B \mathcal{T}\frac{k_z}{\Upsilon} \tag{1}$$

is the parallel (to the magnetic field $\mathbf{B}$) component of the wave vector $\mathbf{k}$. Here, m is the poloidal mode number, k_z is the axial component of $\mathbf{k}$ defined as $k_z = nR_p$ where n is the toroidal mode number and R_p the major radius of the magnetic axis , $\Upsilon = R/R_p$ is a normalized major radius where $R(\psi,\theta) = R_p + r(\psi,\theta)\cos\theta$ is the major radius and $r(\psi,\theta)$ the minor radius at poloidal angle θ and on the surface labeled by the poloidal magnetic flux ψ. At the point (ψ,θ), the angle between the radial direction $\hat{r}$ and $\hat{\psi} = \nabla\psi/\left\|\nabla\psi\right\|$ is α, while $\mathcal{P}\left[\mathcal{T}\right] = B_p\left[B_T\right]/B$ is the normalized poloidal [toroidal] magnetic field whose direction is defined by coefficients σ_I and σ_B which are the signs of the toroidal plasma current and the toroidal magnetic field directions, respectively. According to the chosen convention in C3PO ray tracing code [33], $\sigma_{I,B} = +1$ when toroidal current and magnetic field directions are clockwise and when the tokamak is viewed from the top. It is assumed, like in most experiments, that the LH frequency ω is well above the LH plasma resonance, such that the wave can only couple to the electrons. In this case, warm plasma corrections to the cold dispersion relation may be neglected [8].

The boundaries of the spectral domain into which the LH wave characterized by an initial parallel refractive index $N_{\parallel 0}$ propagates, are determined from the condition $k_\psi = 0$ where $k_\psi = \mathbf{k}\cdot\hat{\psi}$.Calculations here presented are similar to those performed in Ref. [25] , except they are expressed in the general curvilinear system of coordinates used by C3PO ray-tracing and LUKE kinetic solver [33, 34]. From the perpendicular (to the magnetic field $\mathbf{B}$) component of the wave vector $k_\perp^2 = k^2 - k_\parallel^2$, where $k^2 = \mathbf{k}\cdot\mathbf{k}$, they are solutions of the equation

$$N_{\perp,\pm}^2\left(N_\parallel\right) - \left(\frac{N_\parallel - \left(\mathcal{T}/\mathcal{T}_0\right)\left(\Upsilon_0/\Upsilon\right)N_{\parallel 0}}{\mathcal{P}\cos\alpha}\right)^2 - \frac{\Upsilon_0^2}{\Upsilon^2}\frac{N_{\parallel 0}^2}{\mathcal{T}_0^2} + N_\parallel^2 = 0 \tag{2}$$

where zero subscript stands for the initial launching condition of the LH wave at the plasma separatrix. Here, the refractive indexes are defined from the corresponding wave vectors $N_{\perp,\parallel,z} = ck_{\perp,\parallel,z}/\omega$, where ω is the angular frequency of the excited LH wave. Since k_z is a constant of the ray motion because the magnetic configuration is supposed to be axisymmetric, it is determined from the initial condition $m = 0$, using Eq. 1. The labels $(\pm)$ for $N_\perp^2\left(N_\parallel\right)$ identify the slow and fast branches, for which a specific spectral propagation domain must be defined. Both domains share the same lower boundary in $N_\parallel$ when the Stix-Golant condition is satisfied, i.e. if a cold confluence between the two propagating modes exists [36]. This occurs generally when $N_{\parallel 0}$ is slightly greater than $N_{\parallel a} \simeq \sqrt{S} + \sqrt{-D/P}$, where P and S are the Stix representation of the perpendicular and parallel components of the permeability tensor $K_\perp = S$, $K_\parallel = P$, and D is the electromagnetic correction term.

In the electrostatic limit, the dispersion relation simplifies to $N_\perp^2 = -\left(P/S\right)N_\parallel^2$. Neglecting ions contribution, $K_\parallel \simeq -\overline{\omega}_{pe}^2$, where $\overline{\omega}_{pe} = \omega_{pe}/\omega$ and $\omega_{pe} = \sqrt{\left(n_e q_e^2\right)/\left(m_e\varepsilon_0\right)}$ is the electron plasma frequency. Therefore, since $\left(\overline{\omega}_{pe}^2, \overline{\omega}_{ce}^2\right) \gg 1$ and $\overline{\omega}_{pe}^2 \simeq \overline{\omega}_{ce}^2$, where $\overline{\omega}_{ce} = \omega_{ce}/\omega$ is the normalized electron cyclotron frequency, $K_\perp \simeq 1$. Eq. 2 simplifies to

$$\left(\overline{\omega}_{pe}^2\mathcal{P}^2\cos^2\alpha - 1\right)N_\parallel^2 + 2\left(\mathcal{T}/\mathcal{T}_0\right)\left(\Upsilon_0/\Upsilon\right)N_{\parallel 0}N_\parallel - \left(\left(\mathcal{T}/\mathcal{T}_0\right)\left(\Upsilon_0/\Upsilon\right)\right)^2 N_{\parallel 0}^2 = 0 \tag{3}$$

neglecting second order terms in $\mathcal{P}$, since $\mathcal{P} \ll 1$. Its solutions give the boundaries of the spectral propagation domain for the slow wave propagation mode. When the condition

$$\overline{\omega}_{pe}\mathcal{P}\left|\cos\alpha\right| > 1 \tag{4}$$

is fulfilled, Eq. 3 has a single solution corresponding to the lower bound in $N_{\parallel}$. In this case, the upper bound does not exist, and the spectral domain of propagation is open towards high $N_{\parallel}$ values indicating that the LH wave can always reach the resonance condition $N_{\parallel} = N_{\parallel L}$ at which it is strongly absorbed whatever $N_{\parallel 0}$. Conversely, when $\overline{\omega}_{pe}\mathcal{P}\left|\cos\alpha\right| < 1$, Eq. 3 has two roots, and the spectral domain of propagation is fully bounded. This case corresponds to the example illustrated in Fig. 1 for the tokamak TRIAM-1M, in which the spectral propagation domain $\left(N_{\parallel}, R, Z\right)$ is projected onto the equatorial mid-plane at $Z = Z_p$, where Z_p is the vertical position of the magnetic axis. Since the electrostatic approximation holds for the LH wave in TRIAM-1M, i.e. $\omega_{pe}/\omega_{ce} \ll 1$,the solutions of Eq. 3 are very close to those obtained numerically by Eq. 2 using the full electromagnetic dispersion relation. For the simulation here considered, the value $N_{\parallel 0} = 1.96$ is taken, corresponding to the main lobe of the launched power spectrum when antenna phasing is $\triangle\phi = 110\,deg$ between adjacent waveguides, the LH frequency is $f_{LH} = 2.45\,GHz$, the line-averaged electron plasma density is $\tilde{n}_e \simeq 1.7 \times 10^{+18}\,m^{-3}$, the central magnetic field is $B_{T0} = 5\,T$, the toroidal plasma current $I_p = 27\,kA$, and the core electron temperature is $T_{e0} = 1.1\,keV$ as indicated in Ref. [27]. The plasma has an almost circular concentric cross-section. Since the safety factor on the magnetic axis is unknown from data given in Ref. [27], it is arbitrarily set to $q_0 = 3$, with a parabolic radial increase, while its value at the plasma edge is determined from I_p. Conclusions are unchanged if it is lowered down to $q_0 = 1$.

For the HL-2A tokamak, the full electromagnetic dispersion relation must be considered to evaluate the spectral propagation domain regarding the much lower toroidal magnetic field as compared to TRIAM-1M. The boundaries of the spectral propagation domain at $Z = Z_p$ are shown in Figs. 2, 3 and 4 for plasma parameters corresponding to the discharge #35261 at time $t = 0.8\,s$. For this simulation, the main lobe in the launched power spectrum calculated by the ALOHA coupling code for the Passive Active Multi-junction (PAM) is located at $\left|N_{\parallel 0}\right| \simeq 2.95$ [32, 37]. As shown in Sec.3.3, the power spectrum exhibits multiple large satellite lobes. The LH frequency is $f_{LH} = 3.7\,GHz$, the line-averaged electron plasma density is $\bar{n}_e \simeq 0.75 \times 10^{+19}\,m^{-3}$, the central magnetic field is $B_{T0} = 1.3\,T$, the toroidal plasma current $I_p = 127\,kA$, and the core electron temperature estimated by Thomson scattering is $T_{e0} \simeq 2.5\,keV$. The safety factor is obtained from a toroidal MHD equilibrium reconstruction by EFIT code [38]. The case of the satellite lobe at $\left|N_{\parallel 0}\right| = 1.6$ is first considered to illustrate different spectral domain of propagations depending of the type of branch (slow or fast). Both domain boundaries merge when the usual Stix-Golant accessibility condition is fulfilled because of the low refractive index. The same diagram is shown for the main lobe at $\left|N_{\parallel 0}\right| = 2.95$. In this case, as the refractive index is much higher, the usual Stix-Golant accessibility condition does not restrict the lower bound of the propagation domain, and the wave remains on the slow wave branch. Since the upper boundary remains still far from the kinetic resonance domain, $N_{\parallel}$ is bounded and in principle, the LH wave cannot be absorbed in the plasma and drive a toroidal plasma current if this lobe is considered alone. For similar plasma parameters, the spectral propagation domain $\left(N_{\parallel}, R, Z\right)$ projected onto the equatorial mid-plane at $Z = Z_p$ is also presented. The region around $Z = Z_p$ is filled as compared to the propagation domain at $Z = Z_p$ exactly, since more favorable conditions of propagation are encountered near poloidal angle $\theta = \pm\pi/2$, a well-known effect that led to consider mixed low field side and vertical wave launching to localize possibly LH power absorption [39]. In the case of HL-2A, the propagation domain intersects the kinetic domain bounded by $N_{\parallel L}$ because of the high core electron temperature

and high $\left|N_{\|0}\right|$ of the main lobe. Nevertheless, because of the high aspect ratio of the tokamak, the toroidal upshift of $N_{\|}$ is never able to bridge the spectral gap for the main lobe, which carries most of the launched LH power. The close vicinity between the wave propagation domain and the condition of kinetic resonance will lead to consider in detail the role of large satellite lobes in the excited power spectrum to bridge the spectral gap in Sec. 3.3.

As $\mathcal{P} \simeq \left(1+\kappa^2\right)\mathcal{A}^{-1}/\left(2q\right)$, where κ is the plasma ellipticity and $\mathcal{A}$ is the local aspect ratio, the existence of an upper bound for the spectral propagation domain in the electrostatic limit is therefore given approximately by the condition

$$\frac{\omega_{pe}}{\omega}\frac{1+\kappa^2}{2q}\mathcal{A}^{-1}\left|\cos\alpha\right| \ll 1 \tag{5}$$

which depends principally of the magnetic configuration. For high aspect ratio tokamak with circular concentric magnetic flux surfaces for which $\kappa = 0$ and $\left|\cos\alpha\right| = 1$, it is possible to derive a general criterion giving an indication for the existence of an upper bound for the spectral propagation domain. The condition given by Eq. 5 may be recast in a simple form $\gamma_{KAM}^{cyl} g\left(\rho\right) < 1$ where $\max\left(g\right) \simeq 1$ is weakly depending of the current and density profiles in the plasma and γ_{KAM}^{cyl} depends only on main plasma parameters,

$$\gamma_{KAM}^{cyl} = 5.68\frac{I_P\left[MA\right]\sqrt{n_{e0}\left[10^{+19}m^{-3}\right]}}{f_{LH}\left[GHz\right]a_p\left[m\right]B_{T0}\left[T\right]} \tag{6}$$

Consequently, when $\gamma_{KAM}^{cyl} \ll 1$, the spectral propagation domain exhibits an upper limit, while conversely for $\gamma_{KAM}^{cyl} \gg 1$, the spectral domain of propagation is open towards high $N_{\|}$ values. The closer γ_{KAM}^{cyl} is to unity, the higher is the upper bound in $N_{\|}$, such that the existence of an unbridgeable spectral gap may be easily determined for a given electron temperature profile. Since in the electrostatic limit, the roots of Eq. 2 are

$$N_{\|\pm} = \left(\mathcal{T}/\mathcal{T}_0\right)\left(\Upsilon_0/\Upsilon\right)\frac{1 \pm \overline{\omega}_{pe}\mathcal{P}\left|\cos\alpha\right|}{\left(1-\overline{\omega}_{pe}^2\mathcal{P}^2\cos^2\alpha\right)}N_{\|0} \tag{7}$$

when $\overline{\omega}_{pe}\mathcal{P}\left|\cos\alpha\right| \ll 1$, the upper boundary of the propagation domain in $N_{\|}$ in the cylindrical limit with circular concentric magnetic flux surfaces is related to $N_{\|0}$ by the relation

$$N_{\|+} \simeq \left(1+\overline{\omega}_{pe}\mathcal{P}\left|\cos\alpha\right|\right)N_{\|0} \simeq \left(1+\gamma_{KAM}^{cyl}\right)N_{\|0} \tag{8}$$

such that the condition of unbridgeable spectral gap is

$$N_{\|0} \ll \frac{6.5}{\left(1+\gamma_{KAM}^{cyl}\right)\sqrt{\max\left(T_e\left[keV\right]\right)}} \tag{9}$$

which is almost always fulfilled in existing tokamaks, since electron temperature is always too low. Therefore, in general, the condition $\gamma_{KAM}^{cyl} \ll 1$ is sufficient to characterize a bounded spectral domain and an unbridgeable spectral gap.

Though obtained in simplified conditions, this criterion turns out to be rather pertinent even when electromagnetic corrections must be considered as well as for non-circular magnetic flux surfaces. For TRIAM-1M, $\gamma_{KAM}^{cyl} \simeq 0.059$, and the condition of unbridgeable spectral gap is well fulfilled for $N_{\|0} = 1.96$ and $T_{e0} \simeq 1.1\,keV$. For the full LH current drive discharge #35261 performed in the HL-2A tokamak, $\gamma_{KAM}^{cyl} \simeq 0.43$ close to the exact value when electromagnetic corrections are taken into account. For the small lobe in the power spectrum at $\left|N_{\|0}\right| = 1.6$, with $T_{e0} \simeq 2.5\,keV$,

the condition of unbridgeable gap is well fulfilled, as shown in Fig. 2. For the main lobe at $\left|N_{\|0}\right| = 2.95$, that has the dominant contribution to the LH-driven toroidal current, the condition given by inequality (9) is not satisfied, as observed consistently from the propagation domains reported in Fig. 4. In this case, satellites lobes with refractive indexes higher than $\left|N_{\|0}\right|$ may contribute to fill the spectral gap even if the toroidal refraction is inoperative thanks to the large aspect ratio of the magnetic configuration.

From γ_{KAM}^{cyl} and the criterion (9), discharges satisfying the condition of an unbridgeable spectrum gap have been searched in the WEST tokamak database, and only one has been found, corresponding to the discharge #54952 . It corresponds to a discharge where full current drive has been achieved, though transiently because of the rapid onset of a strong MHD activity. As shown in Fig. 5, the spectral gap is very large, whatever the maximum core electron temperature estimated between $1-2\,keV$, as temperature measurements from ECE emission may be overestimated by fast electron pollution, even in the core region of the plasma. Here $\gamma_{KAM}^{cyl} \simeq 0.44$ and the exact value is 0.37. Consistently, from γ_{KAM}^{cyl}, the spectral gap is the largest for plasmas in the TRIAM-1M, while is is comparable for the discharge #54952 in the WEST tokamak and #35261 in the HL-2A tokamak, since aspect ratio of the two latter machines are comparable. Nevertheless, conditions are totally different between WEST and HL-2A, since the spectral gap is much lower in HL-2A, and can be filled by large satellites lobes in the excited power spectrum, a characteristics of LH antenna which will be discussed in Sec. 3.3.

For a given machine, the condition of existence of an unbridgeable spectral gap is not resulting only from the geometrical aspect ratio of the plasma, though this factor deeply contributes to reaching such a regime and even becomes predominant if it is very large like for TRIAM-1M. Indeed, for WEST tokamak discharge #55539, while $\not{A} \simeq 5.6$, at higher toroidal plasma current and electron plasma density, the propagation domain is no more bounded even if the geometrical aspect ratio is unchanged, and the upshift by toroidal refraction may contribute in this case to bridge the spectral gap, as shown in Fig. 6. For this discharge, $\gamma_{KAM}^{cyl} = 1.26$, well above one. The criterion has been also tested for the longest LH-driven discharge #32299 of more than six minutes obtained in Tore Supra tokamak [40]. In the steady-state regime, $\gamma_{KAM}^{cyl} = 0.9$, which means that the propagation domain is almost open. For the nearly full LH current drive discharge #1101104011 in Alcator C-Mod, at time $t = 1.220\,s$, $\gamma_{KAM}^{cyl} = 1.5$ and the propagation domain is effectively fully open towards high $N_{\|}$ values [19]. Finally, for ITER tokamak, thanks to the very high operating current and electron density, $\gamma_{KAM}^{cyl} = 3.2$, a consistent value with the fact that the propagation domain is fully open [41]. As observed, the criterion $\gamma_{KAM}^{cyl} \ll 1$ corresponds well to an unbridgeable spectral gap by toroidal refraction as the wave propagates in the plasma if $\left|N_{\|0}\right|$ is small enough. Since in this case toroidal refraction is intrinsically inoperative, the existence of alternative physical mechanisms contributing to bridge the spectral gap outside the separatrix can be unambiguously identified.

Finally, the impact of the mean aspect ratio $\not{A}$, the electron density and the plasma current have been investigated for the configuration of TRIAM-1M, as shown in Fig. 1. By lowering $\not{A}$ from 7.5 down to 1.13, while all other simulation parameters are kept unchanged, the propagation domain becomes strongly dependent of the major radius and crosses the kinetic domain of absorption on the high magnetic field side (HFS). Even if the propagation domain remains very narrow, the spectral gap can be fully bridged by the toroidal refraction, a result that is consistently supported by ray tracing calculations. Furthermore, as expected from the parametric dependence of γ_{KAM}^{cyl} given by the condition (6), the increase of the electron density or plasma current widen the propagation

domain.

The impact of the LH frequency on the propagation domain has not been investigated explicitly in this work, but increasing f_{LH} clearly helps to lower the upper bound of the propagation domain from Eqs. 4 and 6. Recently the impact of overlapping propagation domains in EAST tokamak for two LH waves injected simultaneously at different frequencies $2.45\,GHz$ and $4.6\,GHz$ has been investigated, based on a similar approach [42, 43].

3. LH current drive simulations

In order to illustrate the impact of the spectral gap on LH current drive in various plasma conditions and for different types of antennas, simulations are performed for the three tokamaks considered in Sec. 2, i.e. TRIAM-1M, WEST and HL-2A. For TRIAM-1M and WEST, the predicted power absorption is negligible if the spectral gap is not filled at the separatrix of the plasma and the calculated LH-driven current and FEB signal are order of magnitudes smaller than experimental observations. This means that the toroidal refraction cannot bridge the spectral gap, as expected from the study of the propagation boundaries and contribute to pull out a tail of fast electrons. To illustrate this fact, the ray propagation for the main lobe in TRIAM-1M is shown in Fig. 7. Corresponding simulations parameters can be found in Sec. 3.1. It is important to note that a possible preexisting tail of runaway electrons that could result from the prior Ohmic phase cannot lead to a continuous absorption of the main lobe at low $\left|N_{\|0}\right|$ in the power spectrum and sustain a steady-state LH current. Indeed, as the LH power is turned on, the Ohmic field drops down quickly, and the accelerating force on the fast electrons vanishes after few collisonal times, especially near the Maxwellian bulk. The spectral gap is consequently fully restored on this time scale, a result that is fully confirmed by kinetic calculations performed with LUKE code. Furthermore, well separated satellite lobes of small amplitudes in the power spectrum, as calculated by ALOHA antenna coupling code for WEST, can never contribute to bridge the spectral gap, since their contributions to the rf-diffusion operator in Fokker-Planck calculations are much too low and furthermore discontinuous, these two characteristics preventing the formation of a supra-thermal electron tail. This statement remains valid when toroidal refraction is weak, even if poloidal positions of the different antenna rows are always considered in the calculations. Therefore, in this case, considering the main lobe alone weighted by the correct antenna directivity or the whole spectrum, as calculated by ALOHA code in RTFP calculations, gives almost identical results.–

When the TSM is considered, it is applied to all lobes of the excited power spectrum considered in the calculations, the main lobe at $\left|N_{\|0}\right|$ but also all considered satellite lobes, whatever their contributions to the plasma current (co- or counter-current). For each lobe, a tail is build which is described by a set of five additional lobes up $N_{\|L}^{\min}$, as shown in Fig. 8. Thanks to the study in Ref. [18], 50 % of the LH power carried by each lobe is transferred to the spectral tail, which guarantee that results are independent of the fraction of power in the tail. Each lobe in the tail corresponds to initial conditions of ray trajectories. The spectral width of each additional lobe is determined to provide a continuity in the power spectrum, thus allowing to build a continuous quasilinear rf-diffusion operator in Fokker-Planck calculations [18]. The amplitude of the lobes in the tail may be constant in $N_{\|}$, or decrease linearly with different slopes. Except if it is explicitly indicated in the text, the slope is chosen to have zero power in the tail at $N_{\|L}^{\min}$, as shown in Fig. 8. Downshift of $\left|N_{\|0}\right|$ is possible in principle, but as it remains very small as shown by full-wave simulations, this effect is always neglected [21].

Even if the wave propagation domain is strongly bounded for HL-2A tokamak like WEST, its close vicinity to the kinetic absorption domain because of the large $\left|N_{\|0}\right|$ of the main lobe and the high core electron temperature make the condition of absorption totally different as compared to the two other machines. In that case, the large satellite lobes which are specific to this type of LH antenna can contribute to fill the much smaller spectral gap as compared to TRIAM-1M and WEST, even if the toroidal upshift is rather weak.

3.1. TRIAM-1M tokamak

TRIAM-1M is a small tokamak characterized by a very large mean aspect ratio, $\not{A} \simeq 7.5$. Its major radius is $R_p = 0.8\,m$ and the minor radius $a = 0.11\,m$. Equipped with superconducting toroidal field magnets, permanent magnetic field up to $6\,T$ can be achieved on axis [27, 29, 44]. Despite its high aspect ratio and while core electron temperature is never exceeding $T_{e0} \simeq 1.0\,keV$, stable steady-state discharges have been successfully achieved by driving all the plasma current $I_p = 35\,kA$ using $P_{LH} = 35\,kW$ of LH power at a frequency of $f_{LH} = 2.45\,GHz$. From fast electron bremsstrahlung measurements, a tail of non-thermal electron centrally peaked is clearly observed, extending up to 60 keV. These results raised the question how a tail of fast electron can be pulled from the bulk in this machine, since the large spectral gap between $N_{\|0}$ and $N_{\|L}^{\min}$ cannot be bridged by toroidal refraction [28]. Since TRIAM-1M tokamak has been dismantled, plasma and LH wave parameters for the simulations have been rebuilt from data in Refs. [27, 45].

According to Brambilla's grill theory [46], $N_{\|0}$ is determined from phase difference $\Delta\phi$ between waveguides by the relation

$$N_{\|0} = \frac{30}{f_{LH}\Delta_w}\frac{\Delta\phi}{2\pi} \tag{10}$$

and the spectral width $\Delta N_{\|0}$ of the lobe at $N_{\|0}$ is

$$\Delta N_{\|0} = \frac{c}{f_{LH}N_{\|0}L_w} \tag{11}$$

where L_w is the full width of the antenna in the toroidal direction. Since the antenna is made of four waveguides spaced by $\Delta_w = 1.9\,cm$ apart, $L_w = 7\,cm$. From Eqs. 10 and 11, values of $N_{\|0}$ and $\Delta N_{\|0}$ are given in Table 2 as function of $\Delta\phi$. Except for $\Delta\phi = 70\,deg$ which corresponds to the main lobe driving co-current at the lowest excited $\left|N_{\|0}\right|$, the condition $\Delta N_{\|0}/\left|N_{\|0}\right| \leq 1$ is well fulfilled for the applicability of the WKB approximation [33, 34]. Satellite lobes at high $\left|N_{\|0}^{cnc}\right|$ driving counter plasma current are taken directly from Ref.[27] and reported in Table 2.

The toroidal magnetic equilibrium for TRIAM-1M is approximated by circular concentric magnetic flux surfaces, a good approximation regarding the large aspect ratio of the magnetic configuration and the low plasma pressure. From Ampere's law, the poloidal field is consistently calculated to retrieve the plasma current I_p, considering a parabolic safety factor profile with $q_0 = 3.0$. It has been shown that lowering q_0 to one does not change simulation results in the regime studied here. Electron density and temperature profiles are described by $n_e\left[T_e\right] = \left(n_{e0}\left[T_{e0}\right] - n_{ea}\left[T_{ea}\right]\right)\left(1-\rho^2\right)^{\alpha_{[n,T]}} + n_{ea}\left[T_{ea}\right]$, where $\rho = [0,1]$ is the normalized minor radius, with $n_{e0}\left[T_{e0}\right]$ and $n_{ea}\left[T_{ea}\right]$ the electron density and temperature in the plasma core at the separatrix respectively. The values of the exponents $\alpha_{[n,T]}$ are $\alpha_T = 1$, $\alpha_n = 0.6$ in order to reproduce the electron temperature profile and the $\left(1-\rho^3\right)$ dependence approximately of the electron density profile that are given in Ref. [27]. In the calculations, $n_{ea} = 0.05 \times n_{e0}$ and n_{e0} are determined to match the indicated line-averaged electron density. The dominant impurity is carbon and its density is determined by assuming that carbon is fully stripped, while the effective charge with a flat profile is $Z_{eff} = 1.6$ in the deuterium plasma. Since current drive efficiency scales approximately as $4/\left(5+Z_{eff}\right)$, results are weakly dependent of the impurity concentration, as far as $Z_{eff} \ll 5$. The ion temperature is $T_i = T_e/2$, as suggested from data in Ref. [27].

Without spectral broadening at the separatrix, the LH wave is unable to drive any current from RTFP calculations, whatever the plasma conditions and $N_{\|0}$ values, consistently with the strongly bounded propagation domain, which prevents resonant interaction with the thermal electronic

population. This result is also consistent with full-wave calculations coupled to a 2-D Fokker-Planck solver in momentum space [20]. Conversely, by considering power spectrum calculated from the TSM, the LH-driven plasma current has the correct order of magnitude as compared to experimental observations. The discharge of reference corresponds to $\Delta_w = 110\,deg$ for which $N_{\|0} = 1.96$ and $\Delta N_{\|0} = 0.82$, $\left|N_{\|0}^{cnc}\right| = 4.0$. Full current drive is achieved with $23\,kW$ of LH power, while the toroidal magnetic field on axis is $B_{t0} = 5\,T$. The core electron temperature for this case is $T_{e0} = 1.1\,keV$, and the line-averaged electron density is $\bar{n}_e = 2.0 \times 10^{+18}\,m^{-3}$. The LH-driven current is $I_{LH} = 144\,kA$, corresponding to a current drive efficiency $\eta = 1.01 \times 10^{+19} AW^{-1}m^{-2}$ three times higher than the experimental one. This difference may be ascribed to some anomalous fast electron radial transport due to natural plasma turbulence in L-mode, since the radial size of the plasma is small and the electron density is low. In this case, radial transport may balance collisional slowing-down, even if the transport remains rather small [47]. In order to retrieve the correct level of the current drive efficiency, an anomalous radial transport for the fast electron population is introduced in the Fokker-Planck calculations. The heuristic form of the diffusion coefficient is $D_{\psi\psi} = D_{\psi\psi 0}\left(v_{\|}/\hat{v}_{th}\right) H\left(v_{\|} - 3.5 \times \hat{v}_{th}\right)$, where $\hat{v}_{th}$ is the thermal velocity at the plasma center and $H\left(x\right)$ the Heaviside function. In the calculations, $D_{\psi\psi 0}$ is taken uniform in the plasma and $D_{\psi\psi} = 0$ when $v_{\|} \leq 3.5 \times \hat{v}_{th}$, such that only fast electrons are concerned by the radial transport. As shown in Fig. 9, the current efficiency η drops down by increasing $D_{\psi\psi 0}$ from 0 to $1.0\,m^2 s^{-1}$, and the value that matches experimental observations corresponds to $D_{\psi\psi 0} = 0.12\,m^2 s^{-1}$, very close to levels found in other LH current drive simulations [2, 18, 19]. Even small, the impact of anomalous radial transport is quite large on the fastest electrons in the LH-driven non-thermal tail thanks to the $v_{\|}$ dependence. This can be evaluated by comparing collisional time τ_c and radial diffusion time τ_D at different electron energies for mean plasma values. It is found that $\tau_c \geq \tau_D$ when kinetic energies of fast electron exceeds $30\,keV$. Therefore, radial diffusion predominates over collisional slowing-down for almost all the supra-thermal tail. As shown in Fig. 10, the current density of the toroidal MHD equilibrium and the calculated one from RTFP calculations have very similar shapes, indicating that the steady-state is effectively achieved with the power spectrum of the tail LH model. Exact match between the two current profiles would require self-consistent toroidal MHD equilibrium with RTFP calculations, which is not the purpose of this work.

Keeping $D_{\psi\psi 0}$ unchanged as well as all plasma parameters, the observed variation of the current drive efficiency η with the waveguide difference of phase $\Delta\phi$ can be well reproduced, as shown in Fig. 11. The agreement concerns not only the relative variation of η, but also the phasing at which the efficiency is maximal. This clearly indicates that first principle calculations have caught most prominent aspects of the LH physics, providing the initial power spectrum at the separatrix is much broader than the excited one by the antenna. Without this spectral broadening, no LH current can be generated with this plasma configuration.

Since ray dynamics for $N_{\|0} = 1.96$ and kinetic calculations are weakly dependent of the toroidal magnetic field in the magnetic configuration of TRIAM-1M (current drive is marginally sensitive to B because the fraction of trapped electrons is also very small when the aspect ratio is large), the rise of the current drive efficiency by increasing B can only be the consequence of a reduction of the anomalous fast radial transport in RTFP calculations. They are performed with $D_{\psi\psi 0}\left(B_{t0}\right) = D_{\psi\psi 0}\left(B_{t0} = 5T\right)\left(5/B_{t0}\right)^{\alpha_B}$ for B values Ref. [27], keeping the same velocity dependence used for the reference discharge corresponding to $B_{t0} = 5\,T$. It is found that $\alpha_B = 2$ gives the best agreement with the estimated LH current efficiency, i.e. that $D_{\psi\psi 0}$ must vary as B^{-2}, a power law which is corresponding to a gyro-Bohm transport scaling (Fig. 12).

Finally, the measured FEB at photon energy $k = 60\,keV$ is centrally peaked and fairly broad

as shown in Refs. [27, 45]. Using HXR diagnostic characteristics given in Ref. [45], it is possible to calculate the FEB at the same energy using the quantum relativistic bremsstrahlung code R5-X2 [35]. As shown, in Fig. 13, the HXR profile is globally well retrieved as well as the correct order of magnitude for the central chords 3-4. However, predictions are much less than observations for chords viewing the outermost part of the plasma region corresponding to $\rho > 0.5$. The disagreement may arise from local underestimation of the anomalous radial transport, thick target HXR back-scattering from the inner wall [48] or higher local density of impurities. The agreement for the central chords can be improved quantitatively by a 15 % increase of the effective charge, a variation of Z_{eff} that has almost no impact on the level of the LH-driven current. By increasing $N_{\|0}$, the calculated photon count rate is slightly decreasing but the HXR profile is not changing, both characteristics that are observed experimentally [45]. Conversely, by decreasing $\left|N_{\|0}\right|$ down to 1.25, the calculated HXR signal is dramatically increasing since resonant fast electrons have a much higher kinetic energy. Surprisingly, an opposite effect is observed experimentally, as indicated in Ref. [45]. It was ascribed to Stix-Golant accessibility, that prevent penetration of very low $N_{\|}$ inside the plasma, an effect which is fully considered in RTFP calculations but which does not appear to be important for TRIAM-1M. It is worth to note that for this very low $\left|N_{\|0}\right|$ value, the condition of applicability of the WKB approximation $\Delta N_{\|0}/\left|N_{\|0}\right| \leq 1$ is not fulfilled [33]. Therefore, the wave propagation cannot be described by ray-tracing, since strong diffraction effects may occur in this case. Moreover, as shown in Refs. [27, 45], the excited power spectrum has no more the characteristics of the usual sinus cardinal function resulting from the Fourier transform of a square box antenna, which raises the question of the validity of the excited power spectrum for this phasing between waveguides. In addition, the existence of a satellite HXR peak at the plasma edge and on the LFS only indicates that non-thermal bremsstrahlung is no more poloidally uniform in this regime, which is beyond codes capability. It may indicate a poloidally and radially localized absorption of the LH wave, as the non-thermal bremsstrahlung extends up to several hundred keV in this region of the plasma. Consequently, the case $\Delta\phi$ is likely strongly anomalous and not pertinent for the overall analysis considered here.

3.2. WEST tokamak discharge #54952

The WEST tokamak, which was primarily designed for studying the impact of Tungsten on the energy transport performances of fusion plasmas and LH current drive in particular, is characterized by a large aspect ratio, $\not{A} \simeq 5.5$, making it potentially attractive for investigating the impact of an unbridgeable gap on the LH wave dynamics. As compared to TRIAM-1M, WEST plasmas have generally a X-point, a property that is known to deeply improve toroidal refraction locally as discussed in Ref. [19]. However, if the spectral gap is unbridgeable, such an effect is inoperative.

In WEST database, very few discharges are satisfying the conditions of an unbridgeable gap, and only one has been identified from the criterion derived in Sec. 2, i.e. discharge #54952, which is particularly interesting, as full current drive is achieved, though transiently because of the rapid onset of a large MHD activity. Nevertheless, much can be learned from the analysis of this shot in the transient quiescent phase, whose main time traces are given in Fig. 14. Indeed, as compared to TRIAM-1M, the fast electron dynamics is expected to be principally dominated by Coulomb collisions (pitch-angle and slowing-down) rather than anomalous radial transport, thanks to the larger size of the plasma while plasma density is much higher. The RTFP analysis is therefore carried out at $t \simeq 4.5s$, just before plasma temperature starts to roll-over, as shown by EC and soft-X-ray emissions, when high-Z impurities remain still at a low level.

At that time, $1\,MW$ of LH power is launched at a frequency of $3.7\,GHz$ by a Fully Active Multi-junction (FAM). Using ALOHA coupling code [32], the excited power spectrum exhibits a high directivity, the main lobe contributing to co-current being peaked at $\left|N_{\|0}\right| = 2.0$, as shown in Fig. 16. Thanks to the spectral characteristics of the LH wave excited by the FAM, the FEB profile is a good proxy of the LH-driven current density profile and not only of the LH power density [6]. Since satellite lobes are very small and far from the main one, they cannot contribute to bridge the spectral gap. Their relative height is slightly sensitive to the density in front of the multi-junction, but the very low level of power that is reflected back to the waveguides (less than 5%) means that the power in the satellite lobes driving counter current drive remains low [6].

While antenna concepts of TRIAM-1M and WEST are totally different - grill or multi-junction, both LH antenna types are able to drive all the plasma current experimentally while boundaries of the propagation domain do not intersect the domain of kinetic resonance, as shown in Figs. 5 and 1. This is an important feature for this particular regime, which indicates that the spectral broadening mechanism between the antenna and the separatrix, that is described by the TSM, is not specific to the type of antenna. This result is discussed in Sec. 4.

In RTFP calculations, only the main lobe of the power spectrum calculated by the antenna coupling code ALOHA is considered, since the power carried by satellite lobes is far too small to force absorption of the main one by resonant wave-particle interaction in Fokker-Planck calculations. Indeed, considering multiple small and well-separated lobes in RTFP calculations do not act like the tail spectral model, and no LH-driven current is predicted by RTFP using the full ALOHA power spectrum, since the associated rf-operator in kinetic calculations is discontinuous, preventing the formation of a tail of fast electrons from the thermal bulk. Conversely, considering few satellites lobes of the power spectrum calculated by the antenna coupling code ALOHA do not change RTFP results if the tail spectral model is taken into account for all of them. Initial ray conditions are obtained assuming a poloidal mode number $m = 0$ [33], and all six rows of waveguides in the poloidal direction are considered in the calculations. Therefore, without any spectral tail, a total of 6 rays are used, while with the TSM, 30 rays must be considered for each simulation.

Calculations are performed using a toroidal MHD equilibrium deduced from time analysis of the discharge using METIS code [49]. The effective charge is large $Z_{eff} \simeq 4$, and impurities considered in the calculations are Helium, Nitrogen, Oxygen and Tungsten. Partial screening effects on collisions are fully considered but remain small at the time slice of this study, either for the LH-driven current or the non-thermal bremsstrahlung. The equilibrium current is $I_p \simeq 300\,kA$, the magnetic field on-axis is $B_{T0} = 3.57\,T$, the internal inductance is $l_i \simeq 1.07$ and safety factor at the plasma center is $q_0 = 2.5$ approximately. The plasma, characterized by a lower single null (LSN) magnetic configuration, as shown in Fig. 15, has an elongation of $\kappa \simeq 1.31$ and a triangularity of $\delta = 0.45$. The Shafranov shift is very small of the order of $2\,cm$, while the main axis major radius is $R_p = 2.55\,m$ and the minor radius is $a_p = 0.46\,m$. The mean aspect ratio is therefore $\not{A} \simeq 5.6$ for this toroidal MHD equilibrium. Electron temperature and density profiles which are obtained from METIS calculations are consistent with magnetic flux consumption. They are as shown in Fig. 17. For the latter, electron line-averaged density is $\bar{n}_e \simeq 1.7 \times 10^{+19} m^{-3}$. In METIS calculations, electron/ion temperature and density as well as impurity content are constrained by measurements. The electron temperature is determined by electron cyclotron emission, and correction from a fast electron pollution of the signal is taken into account. The slight hollowness in the plasma center may arise from a highly radiative core because of local tungsten accumulation, even if the radiated bulk remains globally moderate at the studied time, as shown in Fig. 14,

From RTFP calculations with the TSM model and considering only the main lobe at $\left|N_{\|0}\right| = 2.0$

(tail with a steep slope which is the default case), the calculated LH current is $I_{LH} \simeq 340\,kA$, 10 % larger than the equilibrium current, as well as the calculated internal inductance, $l_i = 1.2$. Without TSM model, the predicted LH current is only $I_{LH} \simeq 1\,kA$. As shown in Fig. 18, the current density profile calculated by RTFP is similar to the current density of the equilibrium, which demonstrate the consistency of the overall calculations. Introducing an anomalous radial transport in RTFP calculations slightly improves the agreement between the two profiles, but this effect remains small as expected. Interestingly, the current density in both profiles exhibit a small maximum around $\rho \simeq 0.2$, which corresponds consistently to the location of the small peak in the electron temperature profile as shown in Fig. 17 This highlight the usual high sensitivity of the LH driven current to the local electron temperature.

The line-integrated fast electron bremsstrahlung profile in the photon interval $60 - 80\,keV$ is shown in Fig. 20. Experimental line-integrated profile is fairly broad with a flat plateau between chords #14 and #26, well symmetric around the central one #21. This corresponds to an hollow local HXR emission profile around $\rho = 0.4$. Beyond the plateau, the HXR emission falls off rapidly, until a minimum is reached at chords #7 and #35 where it increases again, because of the thick target bremsstrahlung on upper and lower targets. Since the magnetic configuration is LSN, signals for chords $\#1 - \#5$ are consistently larger than for those of chords $\#35 - \#49$. Three spectral tails with different slopes (flat, medium and strong) have been considered, as shown in detail in Fig. 19, in order to investigate how the shape of the tail in $N_\parallel$ may impact HXR profiles. For each case, the line-integrated HXR profiles are shown in Fig.20.

As expected, RTFP calculations predict a very small HXR signal without the TSM ($\times 200$ less than observations approximately) and adding few satellite lobes shown in Fig. 16 does not change this result. Interestingly, the predicted line-integrated profile exhibits maxima for chords #14 and #26, close to those observed experimentally. Conversely, with the TSM, the correct level of the experimental HXR signal is globally retrieved, as shown in Fig. 20. In particular, the width of the line-integrated profile is consistently reproduced. By lowering the slope in $N_\parallel$ of the spectral tail, shoulders appear for chords #10 and #31, which are not observed experimentally. This result highlights the great sensitivity of the FEB to the details the power spectrum. For the steepest spectral tail in $N_\parallel$, the signal is narrower than observations, while the corresponding predicted LH current exceed I_p by 15 %, as shown in Fig. 18. This difference may arise from the rather large sensitivity of the HXR emission to the level of impurities. Introducing a small anomalous radial transport with $D_{\psi\psi 0}$ up to $0.3\,m^2 s^{-1}$, as done for TRIAM-1M tokamak in Sec. 3.1, does not change the overall agreement with observations as for the current density profile. Therefore, line-integrated HXR profiles are directly connected to the characteristics of the power spectrum that is absorbed in the plasma. The calculated dependence in photon energy of the FEB is also well reproduced for all chords from $40 - 60\,keV$ up to $100 - 120\,keV$, which represents an important achievement.

Finally, lowering $\left|N_{\parallel 0}\right|$ from 2.0 to 1.8 at fixed input LH power leads to a large excess of LH current, and the HXR signal of central chords is much too high above $100\,keV$ as compared to observations. Therefore, only $\left|N_{\parallel 0}\right| = 2.0$ from ALOHA antenna coupling code gives consistent results, providing the power spectrum is broad at the separatrix with the steepest slope for the TSM.

3.3. HL-2A tokamak discharge #35261

Like TRIAM-1M and WEST machines, HL-2A is a medium size tokamak characterized by a rather large aspect ratio [31]. With the major radius $R = 1.75\,m$ and the minor radius $a = 0.35\,m$,

$\not{A} \simeq 5.0$ during LH current drive experiments, since the plasma is shifted outwards to the LFS in order to minimize the distance between the antenna and the separatrix and improve wave coupling. Interestingly, the toroidal magnetic field is low, $B_T = 1.3\,T$, which restricts drastically the Stix-Golant accessibility and forces to use a higher $\left|N_{\|0}\right|$ which is estimated to 2.95 for the main lobe in order to have better penetration of the LH wave into the plasma core. Consequently, current drive efficiency should be rather low, according to Fisch's current drive theory [9]. Like WEST tokamak, it is equipped with a Passive Active Multi-junction (PAM) operating at the same frequency $f_{LH} = 3.7\,GHz$ with 4 horizontal rows of waveguides grouped in 4 modules per row symmetrically placed in the low field side around the equatorial mid-plane [37]. Full current drive has been achieved in the discharge #35261 by launching $840\,kW$ of LH power [50]. The LH-driven current is $I_p = 127\,kA$, and the line-averaged electron plasma density $\tilde{n}_e \simeq 7.5 \times 10^{+18}\,m^{-3}$. The fairly high core electron temperature is estimated by Thomson scattering to reach $2.5\,keV$ and from detailed comparisons between Ohmic and low power LH discharges, temperature profile can be considered as almost unchanged when LH power is applied.–

Full RTFP simulations have been carried out at time $t = 800\,ms$, first considering the power spectrum calculated by ALOHA antenna coupling code shown in Fig. 21, and selecting the five most prominent satellites lobes for the RT calculations. While toroidal upshift is largely inoperative thanks to the large aspect ratio, most of the LH power is absorbed, which indicates that the spectral gap has been well filled without the TSM, provided $\delta_{N_{\|0}} < 1$. This result is consistent with the smaller spectral gap in HL-2A LH experiments as compared to the two previous machines TRIAM-1M and WEST. In that case, RTFP calculations show that it can be well filled by the rather large satellite lobes at higher $N_{\|}$. This means that the rf-diffusion operator is locally continuous, allowing to pull out a tail a fast electrons from the thermal bulk. Consistently, the HXR line-integrated profiles between $40 - 60\,keV$ are reasonably well reproduced quantitatively, especially for central chords, as shown in Fig. 22, but for the HXR range of photon energy $60 - 80\,keV$, the predicted emission is lower than observations –The predicted LH-driven plasma current is about 60 % lower than the experimental value, with a centrally peaked radial profile. The discrepancy on the plasma current level is likely due to the very low directivity of the LH antenna, as calculated by ALOHA code. In this case, the LH-driven current is highly sensitive to the relative weights between the different lobes, as observed for the same type of antenna in the Tore Supra tokamak [6]. Indeed, any small changes of density in front of the antenna can modify significantly the balance between the amplitudes of the lobes that contribute to drive co- or counter-current. So, accurate LH current calculations are particularly difficult in these conditions.–

When the TSM is considered for the five selected lobes, power absorption is almost unchanged, but the predicted LH-current is increased by 60 % up to $80\,kA$, still lower than the experimental level. The current density remains peaked, and the estimated efficiency is $\eta_{RTFP} \simeq 0.18 \times 10^{+19}(AW^{-1}m^{-2})$, close to the estimated value from the relative drop of the loop voltage when LH power is injected in the plasma, at fixed density and plasma current [50]. Interestingly, time analysis of this discharge using METIS code [49] confirms that LH power absorption must be central with a width of $\Delta\rho = 0.3$ consistent with RTFP calculations, using a current drive efficiency close to η_{RTFP} in order to reproduce observations, as shown in Fig. 24. In both simulations, the predicted internal inductance during LH current drive is significantly larger than in the Ohmic phase ($l_i \sim 3$), a variation that is not observed experimentally, l_i remaining close to unity approximately.–

If the excited power spectrum calculated by ALOHA is rather consistent with observations, while TSM has only a modest contribution in this case, there is no guarantee that the power spectrum at the separatrix is effectively the excited one. Different power spectra used as input

for RT calculations may lead indeed to similar LH current values and HXR profiles.. Therefore, the sensitivity of the calculated LH-current to $\left|N_{\|0}\right|$ has been investigated by considering an ideal single excited lobe $\left|N_{\|0}\right|$ which carries all the launched LH power while the TSM is used to bridge the spectral gap. The antenna directivity is not considered in this case. As shown in Fig. 23, for fixed plasma parameters corresponding to the discharge #35261, the LH-driven current reaches a maximum for $\left|N_{\|0}\right| \simeq 2.6$ around $I_{LH} \simeq 880\,kA$, much higher than the level of the experimental plasma current. At higher $\left|N_{\|0}\right|$ values, I_{LH} drops down rapidly, and for $\left|N_{\|0}\right| \simeq 3.1$, –the predicted LH current is close to the observed one. Nevertheless, since $\left|N_{\|0}\right|$ is high, the energy of the resonant electron is low, and the predicted line-integrated HXR emission profile is twice less than the measured one, while too narrow. Furthermore, the predicted internal inductance is still much too high, around three.–

Therefore, the presence of an anomalous fast electron radial transport is considered, in order to lower the internal inductance and simultaneously broaden the HXR profile. In this case, $\left|N_{\|0}\right| \simeq 2.6$ is considered, which can be, in principle, excited by the PAM antenna with a proper waveguide phasing. The experimental plasma current can be retrieved by introducing an anomalous radial transport of the fast electrons using $D_{\psi\psi 0} \simeq 0.2\,m^2 s^{-1}$ and $D_{\psi\psi} = 0$ when $v_{\|} \leq 3.5 \times \hat{v}_{th}$. In presence of the fast electron radial transport, the HXR line-integrated profiles between $40-60\,keV$ and $60-80\,keV$ can be rather well reproduced quantitatively, in particular for chords at mid-radius as shown in Fig. 22, while the internal inductance is reduced to one, a value very close to the experimental level. Such a result clearly highlights the ambiguity of the regime where the spectral is bridgeable, since many pairs of $\left|N_{\|0}\right|$ and $D_{\psi\psi 0}$ may explain the same experimental observations. To bypass this problem, the LH power spectrum at the separatrix must be measured, which is known to be a very difficult task. Recent attempts have been carried out recently to reach this goal [23, 24]. Finally, it is clearly shown that the PAM LH antenna in HL-2A has a large potential to drive higher plasma current, with an improved efficiency. Phasing study for different target plasmas may help open the operational domain of the LH wave in this machine.–

4. Discussion and conclusions

The well known spectral gap problem of the LH wave in tokamaks has been investigated in a regime where the domain of propagation of the LH wave inside the plasma is strongly bounded in $N_{\parallel}$, thus preventing a large upshift of the LH wave power spectrum as it propagates in the plasma. When the condition of kinetic resonance cannot be fulfilled, no tail of fast electrons can be pulled out from the thermal bulk, and in principle, the LH wave cannot drive any plasma current. Nevertheless, while this regime is unambiguously achieved in the two tokamaks TRIAM-1M and WEST, both characterized by a large aspect ratio, the LH wave is fully able to drive all the plasma current. This paradox raises the question on the physical mechanisms that can bridge the spectral gap, while the usual toroidal refraction is fully inoperative.–

Conversely, for the HL-2A tokamak, since the spectral gap is much lower, it can be filled by the large satellite lobes of the excited power spectrum of the PAM antenna, even if the toroidal upshift is weak, thanks to the large aspect ratio of the machine. In this case, it is not necessary to invoke an extra mechanism to explain the wave absorption, even if the TSM improves slightly the agreement between calculations and observations, as discussed in Ref. [18]. The question of the uniqueness of the set of simulation parameters is also a major difficulty in this regime.–

In order to characterize discharges for which the spectral gap cannot be bridged by toroidal refraction, a general criterion has been derived. If a large geometrical aspect ratio is a key factor to achieve this regime, it can be reinforced by operating at low electron density and low plasma current. Once identified, fully LH-driven plasmas for which the spectral gap is unbridgeable have been simulated using the chain of well benchmarked codes ALOHA [32], C3PO [33], LUKE [34] and R5-X2 [35], allowing quantitative comparisons with experimental observations from first principles. The key diagnostic of this study is the FEB, which is known to give detailed insights on the dynamics of the LH wave and the resonant fast electrons in the plasma [2, 19, 51].

Whatever the machines TRIAM-1M and WEST, calculations predict no driven current by the LH wave, when the toroidal refraction is the single mechanism to bridge the spectral gap. Such a result fully validates the criterion that has been derived to identify this regime. Conversely, if the power spectrum is already broad at the separatrix using the heuristic tail spectral model (TSM), the general features of the non-inductive discharges and moreover some important parametric dependencies can be well reproduced quantitatively for both machines, which represents an important achievement in the understanding of the LH wave physics, and demonstrates unambiguously that alternative physical mechanisms to the toroidal refraction exist and may also fully bridge the spectral gap. The level of agreement is particularly spectacular for TRIAM-1M, while it has the largest aspect ratio. The TSM may be interpreted as a fast fluctuating power spectrum with respect to the collisional slowing-down time [18]. The impact of the characteristics of the tail on the FEB has been clearly shown for the WEST discharge, and the standard shape of the power spectrum at the separatrix where LH power goes to zero at the highest $N_{\parallel}$ value gives the best agreement with observations. This highlights the complex interplay between the dynamics in momentum and radial spaces, even without any anomalous fast electron radial transport.

The multi-machine study has allowed to demonstrate the importance of a spectral broadening to reproduce the experimental phenomenology, whatever the plasma shape, the magnetic field, the initial refractive index of the main lobe in the excited power spectrum, and the type of LH antenna. The mechanism that broaden the initial power spectral is likely universal and from studies carried out in regimes where toroidal refraction could also contribute with a large spectral gap, it has been shown that it can improve substantially the agreement between modeling and measurements [18, 19].

When the spectral gap is small and the excited power spectrum has many lobes of large amplitude close to the main one (in absolute value), as for LH experiments in HL-2A tokamak, broadening the power spectrum at the separatrix improves slightly the agreement between calculations and observations, even if the toroidal upshift is weak. If predictions of the HXR is rather robust, the LH-driven current can be an extremely sensitive quantity, depending of the details of the power spectrum. In this case, its calculation is particularly challenging.

When the TSM is taken into account, all rays are absorbed in almost single pass, despite the existence of a wide gap. The ray-tracing is therefore fully pertinent to model the wave propagation, since all rays are absorbed in single pass, which removes all limitations of the WKB approximations at caustics and cuts-off [33]. Furthermore, the possible rotation of the perpendicular component of the wave vector by density fluctuations, thanks to the local symmetry of the dielectric tensor with respect to the magnetic field [22], has almost no impact on power absorption, since ray lengths are all short. For the same reasons, non-resonant collision absorption is very small. The LH wave is therefore weakly sensitive to plasma perturbations, a feature that has been well observed experimentally, even in presence of a strong MHD activity [3, 52]. The resilience of the LH wave is one of its most important features besides current drive performances.

So far, any broadening in $N_{\|}$ of the excited power spectrum, i.e. along the magnetic field direction, should result from a subtile physical process, since the magnetic field and the electron density are supposed to be constant along magnetic field lines in a tokamak [22]. Since $N_{\|}$ is weakly evolving along ray trajectories that are principally parallel to the toroidal direction, such an effect could only result from diffraction of the wave in the scrape-off layer, very close to the antenna as suggested in Ref. [21]. Moreover, it could not be the consequence of ponderomotive effects, since spectral characteristics of the LH wave turn out to be independent of the input power level. Local measurements of the LH power spectrum at the separatrix would give valuable details about the reality of such a broadening [23, 24].

Alternatively, the broadening in $N_{\|}$ may be viewed as just an artifact to by-pass intrinsic limitations of the rf diffusion operator that is used in most Fokker-Planck calculations [53, 54], and force to build a broader and continuous quasilinear operator in momentum space on each magnetic flux surface. Indeed, the quasilinear approach may be inadequate for commonly used LH power as indicated in Refs. [55, 56], since at high electric field amplitudes, the interaction region between the electrons and the oscillating electric field can become significantly broader than the quasilinear resonant region. Therefore, the usual picture of the spectral gap may be inappropriate, whatever the input power spectrum. Some indications that support this possible interpretation is the universality of the TSM on one side, and the better qualitative agreement (to a factor $\times 200$) with measured and calculated FEB for the studied WEST full current drive discharge, when only the main lobe at low $\left|N_{\|0}\right|$ is considered, on the other side. If this interpretation is confirmed, the kinetic absorption of the LH wave should be deeply revisited in Fokker-Planck codes, because of the inapplicability of the Landau damping rate and the non-diffusive character of the interaction between electrons and the LH wave.

Acknowledgments

This work has been carried out within the framework of the EUROfusion Consortium and has received funding from the European research and training programme under grant agreement N° 633053. The views and opinions expressed herein do not necessarily reflect those of the European Commission. The LHCD experiments on HL-2A was supported by the Natural Science Foundation of China (NSFC) project (No. 11575054). This work was supported by the HARMONIA Grant nr 2018/30/M/ST2/00799 and PL-Grid Infrastructure.

References

[1] P. T. Bonoli. Review of recent experimental and modeling progress in the lower hybrid range of frequencies at iter relevant parameters. *Phys. Plasmas*, 21:061508, 2014.

[2] Y. Peysson, P. T. Bonoli, J. Chen, A Garofalo, J. Hillairet, M. Li, J. Qian, S. Shiraiwa, J. Decker, B. J. Ding, A. Ekedahl, M. Goniche, and X. Zhai. Current challenges in the first principle quantitative modelling of the lower hybrid current drive in tokamaks. *EPJ Web of Conferences*, 157:02007, 2017.

[3] Y. Peysson and the TORE SUPRA Team. Progress towards high-power lower hybrid current drive in TORE SUPRA. *Plasma Phys. Control. Fusion*, 42(12B):87–114, 2000.

[4] O. Barana, D. Mazon, L. Laborde, and F. Turco. Feedback control of the lower hybrid power deposition profile on tore supra. *Plasma Phys. Control. Fusion*, 49:947–967, 2007.

[5] A. Schmidt, P. T. Bonoli, O. Meneghini, R. R. Parker, M. Porkolab, S. Shiraiwa, G. Wallace, J. C. Wright, R. W. Harvey, and J. R. Wilson. Investigation of lower hybrid physics through power modulation experiments on alcator c-mod. *Phys. Plasmas*, 18:056122, 2011.

[6] E. Nilsson, J. Decker, Y. Peysson, J.-F. Artaud, A. Ekedahl, J. Hillairet, T. Aniel, V. Basiuk, M. Goniche, F. Imbeaux, D. Mazon, and P. Sharma. Comparative modelling of lower hybrid current drive with two launcher designs in the tore supra tokamak. *Nucl. Fusion*, 53:083018, 2013.

[7] R. T. Mumgaard. *Lower Hybrid Current Drive on Alcator C-Mod: Measurements with an Upgraded MSE Diagnostic and Comparisons to Simulation.* PhD thesis, MASSACHUSETTS INSTITUTE OF TECHNOLOGY, 2015.

[8] P.T. Bonoli. Linear theory of lower hybrid heating. *IEEE Trans. on Plasma Sci.*, PS-12(2):95–107, 1984.

[9] N.J. Fisch. Theory of current drive in plasmas. *Rev. Mod. Phys.*, 59(1):175–234, 1987.

[10] Yu. F. Baranov and V. I. Fedorov. Ray-tracing for lower-hybrid waves in a tokamak. *Sov. Tech. Phys. Letters*, 4(7):322–323, 1978.

[11] P.T. Bonoli and R.C. Englade. Simulation model for lower hybrid current drive. *Phys. Fluids*, 29(9):2937–2950, 1986.

[12] J. C. Wright, P. T. Bonoli, M. Brambilla, F. Meo, E. D'Azevedo, D. B. Batchelor, E. F. Jaeger, L. A. Berry, C. K. Phillips, and A. Pletzer. Full wave simulations of fast wave mode conversion and lower hybrid wave propagation in tokamaks. *Phys. Plasmas*, 11:2473–2479, 2004.

[13] J. C. Wright, P. T. Bonoli, A. E. Schmidt, C. K. Phillips, E. J. Valeo, R. W. Harvey, and M. A. Brambilla. An assessment of full wave effects on the propagation and absorption of lower hybrid waves. *PHYSICS OF PLASMAS*, 16(7), 2009.

[14] A. S. Richardson, P. T. Bonoli, and J. C. Wright. The lower hybrid wave cutoff: A case study in eikonal methods. *Phys. Plasmas*, 17:052107–052118, 2010.

[15] P. T. Bonoli and E. Ott. Toroldal and scattering effects on lower-hybrid wave propagation. *Phys. Fluids*, 25(2):359–375, 1982.

[16] J. P. Bizarro and D. Moreau. On ray stochasticity during lower hybrid current drive in tokamaks. *Phys. Fluids B*, 5(4):1227–1238, 1993.

[17] J.P. BIZARRO. On the dynamics of the launched power spectrum during lower hybrid current drive in tokamaks. *Nucl. Fusion*, 33:831–834, 1993.

[18] J. Decker, Y. Peysson, J.-F. Artaud, E. Nilsson, A. Ekedahl, M. Goniche, J. Hillairet, and D. Mazon. Damping of lower hybrid waves in large spectral gap configurations. *Phys. Plasmas*, 21:092504, 2014.

[19] Y. Peysson, J. Decker, E. Nilsson, J. F. Artaud, A. Ekedahl, M. Goniche, J. Hillairet, B. Ding, M. Li, P. T. Bonoli, S. Shiraiwa, and M. Madi. Advances in modeling of lower hybrid current drive. *Plasma Phys. Control. Fusion*, 58:044008, 2016.

[20] Y. Peysson, E. Sébelin, X. Litaudon, D. Moreau, J. C. Miellou, M. Shoucri, and I. P. Shkarofsky. Full wave modelling of the lower hybrid current drive in tokamaks. *Nucl. Fusion*, 38(6):939–944, 1998.

[21] M. Madi, Y. Peysson, J. Decker, and K. Y. Kabalan. Propagation of the lower hybrid wave in a density fluctuating sol. *Plasma Phys. Control. Fusion*, 57:125001, 2015.

[22] Y Peysson, J Decker, L Morini, and S Coda. Rf current drive and plasma fluctuations. *Plasma Phys. Control. Fusion*, 53:124028, 2011.

[23] E.H. Martin, C. Lau, G.M. Wallace, S. Shiraiwa, and R.T. Mumgaard. Experimental evidence of lower hybrid wave scattering in alcator c-mod due to scrape off layer density fluctuations. *Nucl. Fusion*, 59:076006, 2019.

[24] C. Lau, E.H. Martin, S. Shiraiwa, and G.M. Wallace. Full-wave model for the lower hybrid wave electric field vector with synthetic turbulence on alcator c-mod. *Nucl. Fusion*, 60:036001, 2020.

[25] F. PAOLETTI, D.W. IGNAT, J. KESNER, S. BERNABEI, R. KAITA, B. LEBLANC, F.M. LEVINTON, and S.C. LUCKHARDT. Lower hybrid current drive accessibility study with reconstructed magnetic equilibria in pbx-m. *Nucl. Fusion*, 34:771–776, 1994.

[26] E. Barbato. The role of non-resonant collision dissipation of lower hybrid current driven plasmas. *Nucl. Fusion*, 51:103032, 2011.

[27] S. MORIYAMA, Y. NAKAMURA, A. NAGAO, E. JOTAKI, K. NAKAMURA, N. HIRAKI, and S. ITOH. Ultra-long pulse operation using lower hybrid waves on the superconducting high field tokamak triam-1m. *Nucl. Fusion*, 30:47–57, 1990.

[28] H. Takahashi. The generalized accessibility and spectral gap of lower hybrid waves in tokamaks. *Phys. Plasmas*, 1(7):2254–2276, 1994.

[29] H. Zushi, S. Itoh, K. Hanada, K. Nakamura, M. Sakamoto, E. Jotaki, M. Hasegawa, Y.D. Pan, S.V. Kulkarni, A. Iyomasa, S. Kawasaki, H. Nakashima, N. Yoshida, K. Tokunaga, T. Fujiwara, M. Miyamoto, H. Nakano, M. Yuno, A. Murakami, S. Nakamura, N. Sakamoto, K. Shinoda, S. Yamazoe, H. Akanishi, K. Kuramoto, Y. Matsuo, A. Iwamae, T. Fuijimoto, A. Komori, T. Morisaki, H. Suzuki, S. Masuzaki, Y. Hirooka, Y. Nakashima, and O. Mitarai. Overview of steady state tokamak plasma experiments in triam-1m. *Nucl. Fusion*, 43:1600–1609, 2003.

[30] C. Bourdelle, J.F. Artaud, V. Basiuk, M. Becoulet, S. Bremond, J. Bucalossi, H. Bufferand, G. Ciraolo, L. Colas, Y. Corre, X. Courtois, J. Decker, L. Delpech, P. Devynck, G. Dif-Pradalier, R.P. Doerner, D. Douai, R. Dumont, A. Ekedahl, N. Fedorczak, C. Fenzi, M. Firdaouss, J. Garcia, P. Ghendrih, C. Gil, G. Giruzzi, M. Goniche, C. Grisolia, A. Grosman, D. Guilhem, R. Guirlet, J. Gunn, P. Hennequin, J. Hillairet, T. Hoang, F. Imbeaux, I. Ivanova-Stanik, E. Joffrin, A. Kallenbach, J. Linke, T. Loarer, P. Lotte, P. Maget, Y. Marandet, M.L. Mayoral, O. Meyer, M. Missirlian, P. Mollard, P. Monier-Garbet, P. Moreau, E. Nardon, B. Pegourie, Y. Peysson, R. Sabot, F. Saint-Laurent, M. Schneider, J.M. Travere, E. Tsitrone, S. Vartanian, L. Vermare, M. Yoshida, R. Zagorski, and JET Contributors. West physics basis. *Nucl. Fusion*, 55:063017, 2015.

[31] Y. Liu, X.T. Ding, Q.W. Yang, L.W. Yan, D.Q. Liu, W.M. Xuan, L.Y. Chen, X.M. Song, Z. Cao, J.H. Zhang, W.C. Mao, C.P. Zhou, X.D. Li, S.J. Wang, J.C. Yan, M.N. Bu, Y.H. Chen, C.H. Cui, Z.Y. Cui, Z.C. Deng, W.Y. Hong, H.T. Hu, Y. Huang, Z.H. Kang, B. Li, W. Li, F.Z. Li, G.S. Li, H.J. Li, Q. Li, Y.G. Li, Z.J. Li, Yi Liu, Z.T. Liu, C.W. Luo, X.H. Mao, Y.D. Pan, J. Rao, K. Shao, X.Y. Song, M. Wang, M.X. Wang, Q.M. Wang, Z.G. Xiao, Y.F. Xie, L.H. Yao, L.Y. Yao, Y.J. Zheng, G.W. Zhong, Y. Zhou, and C.H. Pan. Recent advances in the hl-2a tokamak experiments. *Nucl. Fusion*, 45:S239–S244, 2005.

[32] J. Hillairet, D. Voyer, A. Ekedahl, M. Goniche, M. Kazda, O. Meneghini, D. Milanesio, and M. Preynas. Aloha: an advanced lower hybrid antenna coupling code. *Nuclear Fusion*, 50(12):125010, 2010.

[33] Y. Peysson, J.Decker, and L. Morini. A versatile ray-tracing code for studying rf wave propagation in toroidal magnetized plasmas. *Plasma Phys. Control. Fusion*, 54:045003 (16pp), 2012.

[34] Y. PEYSSON and J. DECKER. Numerical simulations of the radio-frequency driven toroidal current in tokamaks. *Fusion Science and Technology*, 65:22–42, 2014.

[35] Y. Peysson and J. Decker. Fast electron bremsstrahlung in axisymmetric magnetic configuration. *Phys. Plasmas*, 15(9):092509, 2008.

[36] M. Brambilla. *Kinetic Theory of Plasma Waves*. Oxford Science Publications, 1998.

[37] XingYu Bai, Bo Lu, Hao Zeng, Jun Liang, Chao Wang, GuoLiang Xiao, He Wang, YaLi Chen, JieQiong Wang, Kun Feng, ShaoDong Song, Mei Huang, Jun Rao, XianMing Song, Rui Mao, Jun Cheng, YiPo Zhang, DeLiang Yu, Yan Zhou, ZhongBing Shi, Annika Ekedahl, Julien Hillairet, Emmanuel Bertrand, Lena Delpech, Gerardo Giruzzi, Tuong Hoang, Roland Magne, Didier Mazon, Yves Peysson, XiaoLan Zou, and the HL-2A Team. Development and application of 3.7ghz lhcd system on hl-2a and development of rf heating system on hl-2m. *EPJ Web of Conferences*, 157:02001, 2017.

[38] L. L. LAO, H. E. ST. JOHN, Q. PENG, J. R. FERRON, E. J. STRAIT, T. S. TAYLOR, W. H. MEYER, C. ZHANG, and K. I. YOU. Mhd equilibrium reconstruction in the diii-d tokamak. *FUSION SCIENCE AND TECHNOLOGY*, 48:968–977, 2005. EFIT reference.

[39] S. Ide, O. Naito an d T. Kondoh, Y. Ikeda, and K. Ushigusa. Enhancement of absorption of lower hybrid wave by filling the spectral gap. *Phys. Rev. Letters*, 73(17):2312 – 2315, 1994.

[40] D. van Houtte, G. Martin, A. Bécoulet, J. Bucalossi, F. Saint-Laurent, B. Saoutic, and X. Tore supra team. Real time control of fully non-inductive operation in tore supra leading to 6 min, 1 gj plasma discharges. *Fusion Eng. and Design*, 74:651–658, 2005.

[41] J. Decker, Y. Peysson, J. Hillairet, J.-F. Artaud, V. Basiuk, A. Becoulet, A. Ekedahl, M. Goniche, G.T. Hoang, F. Imbeaux, A.K. Ram, and M. Schneider. Calculations of lower hybrid current drive in iter. *Nucl. Fusion*, 51:073025, 2011.

[42] X M Zhai, N Xiang, J L Chen, P T Bonoli, S Shiraiwa, A M Garofalo, C Yang, M H Li, J P Qian, G Q Li, K Li, H Q Liu, B Lyu, and Q Zang. Theoretical analysis of key factors achieving reversed magnetic shear q-profiles sustained with lower hybrid waves on east. *Plasma Phys. Control. Fusion*, 61:045002, 2019.

[43] X. M. Zhai, J. L. Chen, N. Xiang, P. T. Bonoli, and S. Shiraiwa. Synergy of two lower hybrid waves with different frequencies on east. *Phys. Plasmas 26*, 26:052509, 2019.

[44] S. Itoh, Y. Nakamura, N. Hiraki, K. Nakamura, A. Nagao, S. Moriyama, and and E. Jotaki S. Kawasaki. Initial operation of the high field superconducting tokamak triam-1m. *Plasma Physics and Controlled Nuclear Fusion Research,*, 3:321, 1986.

[45] Y. NAKAMURA, Y. TAKABATAKE, E. JOTAKI, S. MORIYAMA, A. NAGAO, K. NAKAMURA, N. HIRAKI, and S. ITOH. Radial profiles of hard x-ray emission during steady state current drive in the triam-1m tokamak. *Nucl. Fusion*, 30:689, 1990.

[46] G. Tonon. Heating and current drive by lh-waves on toroidal plasmas: problems and perspectives. *Plasma Phys. Control. Fusion*, 26:145–155, 1984.

[47] Y. Peysson. Transport of fast electrons during lhcd in ts, jet and asdex. *Plasma Phys. Control. Fusion*, 35(12B):B253–B262, 1993.

[48] Y. Peysson, P. Froissard, and C. Pocheau. Study of radiation scattering in the hard X-ray energy range by a tokamak inner wall. *Nucl. Fusion*, 33(8):1133–1145, 1993.

[49] J.F. Artaud, F. Imbeaux, J. Garcia, G. Giruzzi, T. Aniel, V. Basiuk, A. B A©coulet, C. Bourdelle, Y. Buravand, J. Decker, R. Dumont, L.G. Eriksson, X. Garbet, R. Guirlet, G.T. Hoang, P. Huynh, E. Joffrin, X. Litaudon, P. Maget, D. Moreau, R. Nouailletas, B. PÃ©gouri A©, Y. Peysson, M. Schneider, and J. Urban. Metis: a fast integrated tokamak modelling tool for scenario design. *Nuc. Fusion*, 58:105001, 2018.

[50] B. Lu, X.Y. Bai, Y. Peysson, Y.P. Zhang, D. Mazon, G.L. Xiao, X.L. Zou, H. Zeng, J. Liang, C.Wang, Y.L. Chen, A. Ekedahl, L. Delpech, J.Q. Wang, K. Feng, H. Wang, J. Rao, B Li, S Wang, X.M. Song, J. Cheng, Y. Zhou, Z.B. Shi, J. Hillairet, E. Bertrand, G. Giruzzi, and T. Hoang. Recent lhcd experiments on hl-2a and lhcd system development on hl-2m. In *Proc. of the 23rd Topical Conference on Radiofrequency Power in Plasmas (Hefei, China)*, 2019.

[51] P. T. Bonoli, J. Ko, R. Parker, A. E. Schmidt, G. Wallace, J. C. Wright, C. L. Fiore, A. E. Hubbard, J. Irby, E. Marmar, M. Porkolab, D. Terry, S. M. Wolfe, S. J. Wukitch, the Alcator C-Mod Team, and J. R. Wilson a. Lower hybrid current drive experiments on alcator c-mod: Comparison with theory and simulation. *Phys. Plasmas*, 15:056117 (1–13), 2008.

[52] Y. Peysson and the Tore Supra Team. High power lower hybrid current drive experiments in the tore supra tokamak. *Nucl. Fusion*, 41(11):1703–1713, 2001.

[53] C.F. Kennel and F. Engelmann. Velocity space diffusion from weak plasma turbulence in a magnetic field. *Phys. Fluids*, 9(12):2377–2387, 1966.

[54] I. Lerche. Quasilinear theory of resonant diffusion in a magneto-active relativistic plasma. *Phys. Fluids*, 11(8):1720–1726, 1968.

[55] P. Pavlo and L. Krlin. Limits of applicability of the quasilinear approximation to the lower hybrid wave-plasma interaction. *Plasma Phys. Control. Fusion*, 41:541–550, 1999.

[56] L Krlin, P Pavlo, R Panek, R Klima, and V Petrzilka. Nonlinear effects in lh wave-plasma interaction. *Plasma Phys. Control. Fusion*, 44:159–170, 2002.

Tokamak	TRIAM-1M	WEST	HL-2A
$R_p\,[m]$	0.8	2.55	1.75
$a_p\,[m]$	0.11	0.46	0.35
Aspect ratio	7.5	5.6	5.0
$B_{T0}\,[T]$	6.00	3.57	1.3
$I_p\,[kA]$	35	300	127
$\bar{n}_e\,\left[10^{+19}\,m^{-3}\right]$	0.2	1.7	0.75
Antenna type	grill	FAM	PAM
$f_{LH}\,[GHz]$	2.45	3.7	3.7
$P_{LH}\,[kW]$	35	1000	840

Table 1. Table of main simulation parameters. Details and more data are given in the main text.

$\Delta\phi$ $(deg.)$	$N_{\parallel 0}$	$\Delta N_{\parallel 0}$	$\boxed{N_{\parallel 0}^{cnc}}$
70	1.25	1.28	4.50
90	1.61	1.00	4.50
110	1.96	0.82	4.00
130	2.32	0.69	3.80
150	2.68	0.60	3.80

Table 2. Table of $N_{\parallel 0}$ and $\Delta N_{\parallel 0}$ as function of the phase difference $\Delta\phi$ between waveguides for LH antenna in TRIAM-1M tokamak. $N_{\parallel 0}^{cnc}$ corresponds to the lobe of the launch power spectrum driving counter-current as shown in Ref. [27].

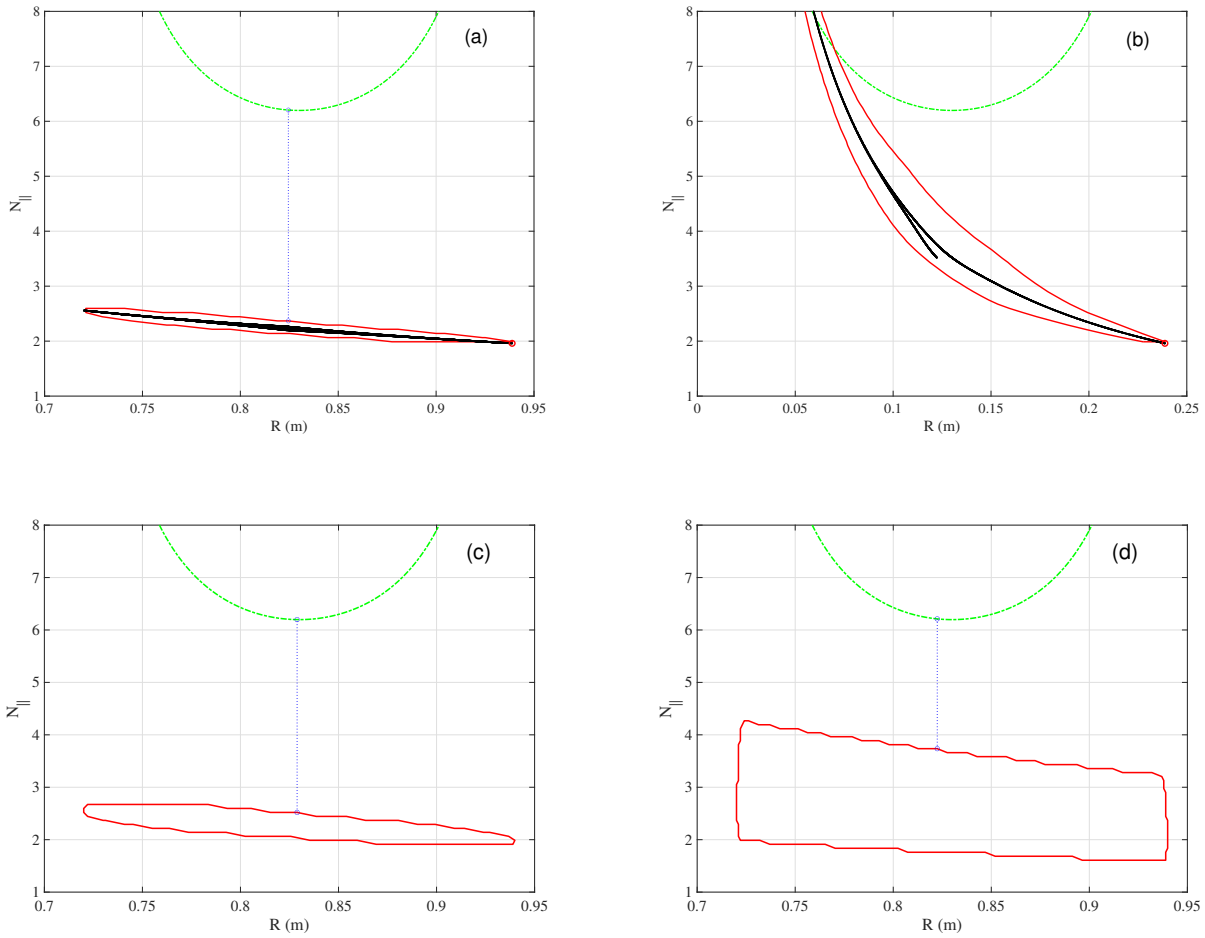

Figure 1. (a) Red full line: propagation domain $\left(R, Z, N_{\|}\right)$ for $N_{\|0} = 1.96$ projected on $\left(R, Z = Z_p, N_{\|}\right)$ space for the LH wave in the TRIAM-1M tokamak calculated using the full electromagnetic cold dispersion relation. The aspect ratio is $\mathcal{A} = 7.5$. Blue dots correspond to the propagation domain determined from the analytical solutions of Eq. 3 in the electrostatic limit which holds for this tokamak. The line-averaged plasma density is $\tilde{n}_e \simeq 1.7 \times 10^{+18}\, m^{-3}$, the central magnetic field is $B_{T0} = 5\, T$, the toroidal plasma current is $I_p = 27\, kA$, according to Ref. [27] and the central safety factor is taken to $q_0 = 3$. Black line: corresponding ray trajectory calculated by C3PO code [33]. The red circle highlights the ray starting point [33]. Green dashed curve: kinetic domain of strong linear absorption for the LH wave characterized by the condition $N_{\|} = N_{\|L}$. The core electron temperature is $T_{e0} = 1.1\, keV$ [27]; (b) aspect ratio has been reduced down to 1.18, all other parameters being unchanged as compared to TRIAM-1M case; (c) the electron density has been increased by a factor 4, all other parameters being unchanged as compared to TRIAM-1M case; (d) plasma current has been increased by a a factor 18, all other parameters being unchanged as compared to TRIAM-1M case.

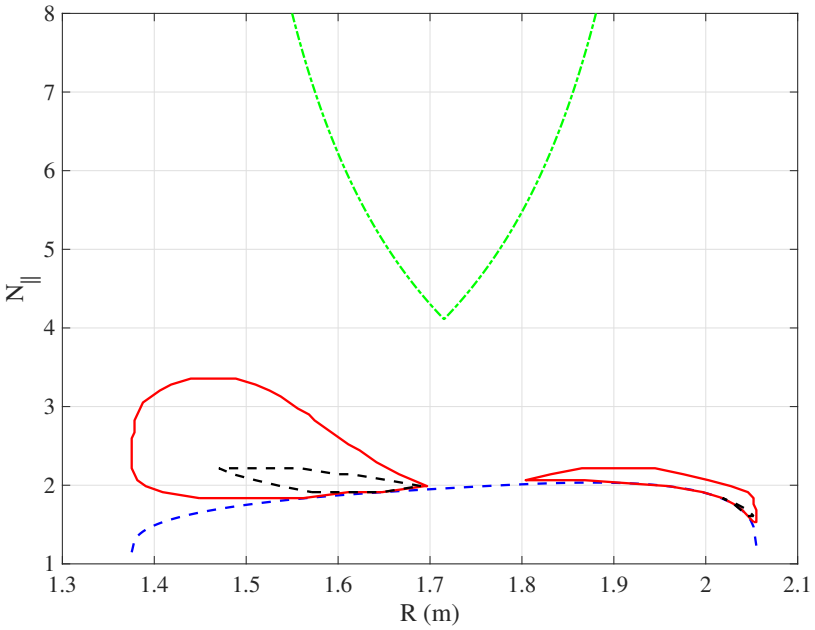

Figure 2. Red full line: slow wave propagation domain $(R, N_\parallel)$ at $Z = Z_p$ for $|N_{\parallel 0}| = 1.6$ for the LH wave in the HL-2A tokamak calculated using the full electromagnetic dispersion relation. Black dashed line: fast wave propagation domain $(R, N_\parallel)$ at $Z = Z_p$ for $|N_{\parallel 0}| = 1.6$. Blue dashed line: Stix-Golant $N_{\parallel a}$ accessibility boundary corresponding to the cold confluence between slow and fast wave propagation modes. When it takes place, both slow and fast wave propagation boundaries merge to $N_{\parallel a}$. Green dashed curve: kinetic domain of strong linear absorption for the LH wave characterized by the condition $N_\parallel = N_{\parallel L}$. The line-averaged plasma density is $\tilde{n}_e \simeq 7.5 \times 10^{+18}\, m^{-3}$, the central magnetic field is $B_{T0} = 1.3\, T$, the toroidal plasma current is $I_p = 127\, kA$ and the central safety factor is taken to $q_0 = 1.5$. The core electron temperature is $T_{e0} = 2.5\, keV$. Plasma and RF wave parameters correspond to the fully driven LH discharge #35261 at $t = 800\, ms$. $|N_{\parallel 0}| = 1.6$ corresponds to a satellite lobe in the launched power spectrum.

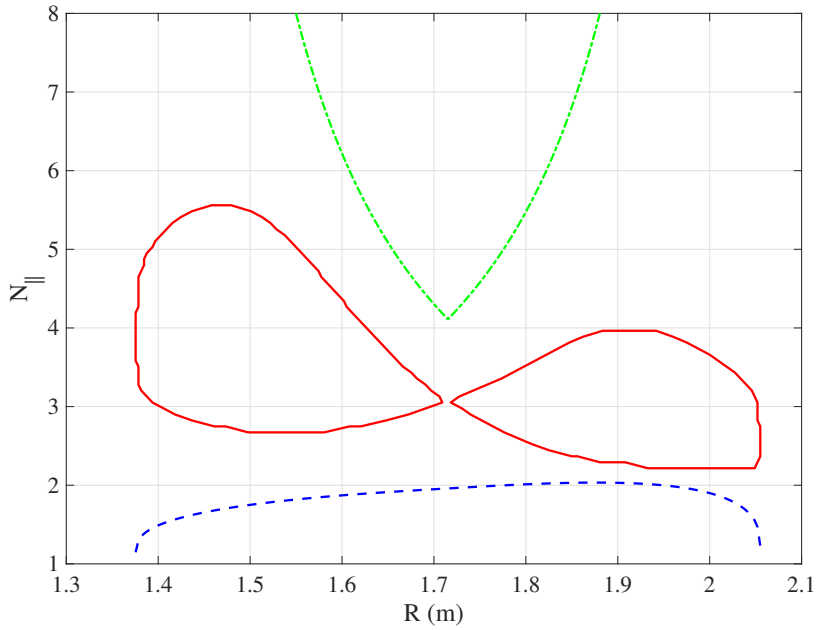

Figure 3. Red full line: slow wave propagation domain $(R, N_\parallel)$ at $Z = Z_p$ for $|N_{\parallel 0}| = 2.95$ for the LH wave in the HL-2A tokamak calculated using the full electromagnetic dispersion relation. Black dashed line: fast wave propagation domain $(R, N_\parallel)$ at $Z = Z_p$ for $|N_{\parallel 0}| = 2.95$. Blue dashed line: Stix-Golant $N_{\parallel a}$ accessibility boundary corresponding to the cold confluence between slow and fast wave propagation modes. When it takes place, both slow and fast wave propagation boundaries merge to $N_{\parallel a}$. Green dashed curve: kinetic domain of strong linear absorption for the LH wave characterized by the condition $N_\parallel = N_{\parallel L}$. The line-averaged plasma density is $\tilde{n}_e \simeq 7.5 \times 10^{+18}\, m^{-3}$, the central magnetic field is $B_{T0} = 1.3\, T$, the toroidal plasma current is $I_p = 127\, kA$ and the central safety factor is taken to $q_0 = 1.5$. The core electron temperature is $T_{e0} = 2.5\, keV$. Plasma and RF wave parameters correspond to the fully driven LH discharge #35261 at $t = 800\, ms$. $|N_{\parallel 0}| = 2.95$ corresponds to the main lobe in the launched power spectrum.

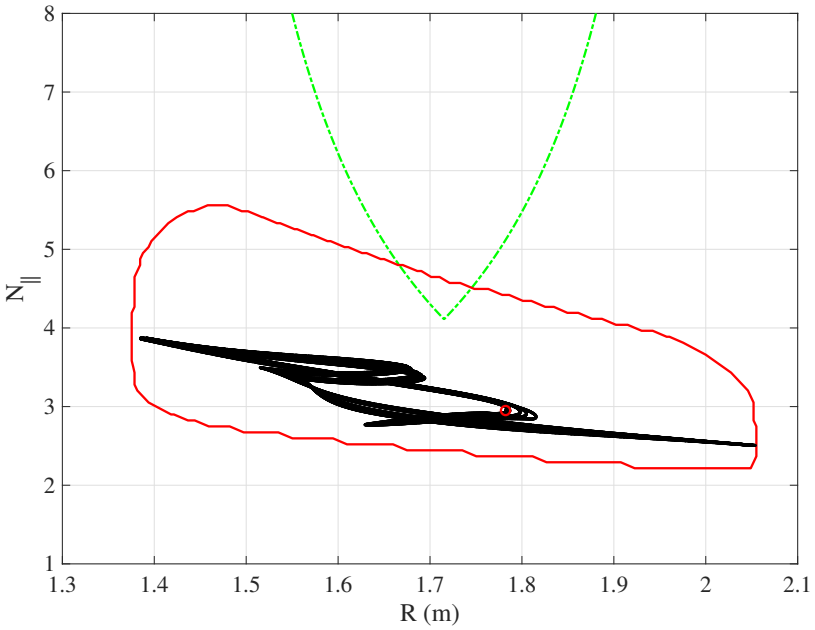

Figure 4. Red full line: propagation domain $\left(R, Z, N_{\parallel}\right)$ for $\left|N_{\parallel 0}\right| = 2.95$ projected on $\left(R, Z = Z_p, N_{\parallel}\right)$ space for the LH wave in the HL-2A tokamak calculated using the full electromagnetic dispersion relation. The line-averaged plasma density is $\tilde{n}_e \simeq 7.5 \times 10^{+18}\, m^{-3}$, the central magnetic field is $B_{T0} = 1.3\, T$, the toroidal plasma current is $I_p = 127\, kA$, according to Ref. [27] and the central safety factor is taken to $q_0 = 1.5$. Black line: corresponding ray trajectory calculated by C3PO code. The red circle highlights the ray starting point [33]. Green dashed curve: kinetic domain of strong linear absorption for the LH wave characterized by the condition $N_{\parallel} = N_{\parallel L}$. The core electron temperature is $T_{e0} = 2.5\, keV$. Plasma and RF wave parameters correspond to the fully driven LH discharge #35261 at $t = 800\, ms$. $\left|N_{\parallel 0}\right| = 2.95$ corresponds to the main lobe in the launched power spectrum.

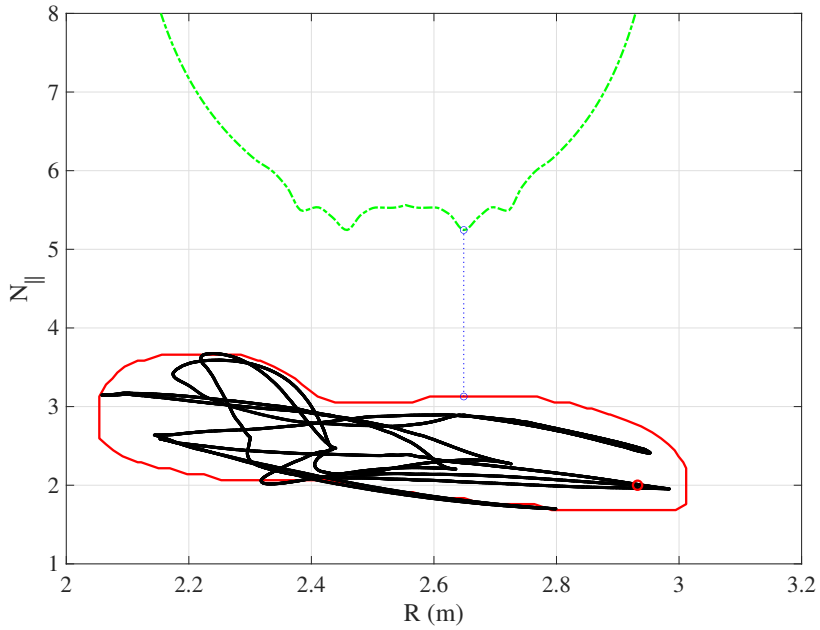

Figure 5. Red full line: propagation domain $(R, Z, N_\parallel)$ for $|N_{\parallel 0}| = 2.0$ projected on $(R, Z = Z_p, N_\parallel)$ space for the LH wave in the WEST tokamak calculated using the full electromagnetic dispersion relation. The line-averaged plasma density is $\bar{n}_e \simeq 1.7 \times 10^{+19}\, m^{-3}$, the central magnetic field is $B_{T0} = 3.57\, T$, the toroidal plasma current is $I_p = 300\, kA$ and the central safety factor is $q_0 \simeq 2.5$. Black line: corresponding ray trajectory calculated by C3PO code. The red circle highlights the ray starting point [33]. Green dashed curve : kinetic domain of strong linear absorption for the LH wave characterized by the condition $N_\parallel = N_{\parallel L}$. Core electron temperatures is $T_{e0} \simeq 1.5\, keV$. Plasma and RF wave parameters correspond to the fully driven LH discharge #54952 at $t = 4.5\, s$ where the main lobe in the launched power spectrum calculated by ALOHA antenna coupling code is at $|N_{\parallel 0}| \simeq 2.0$ [32].

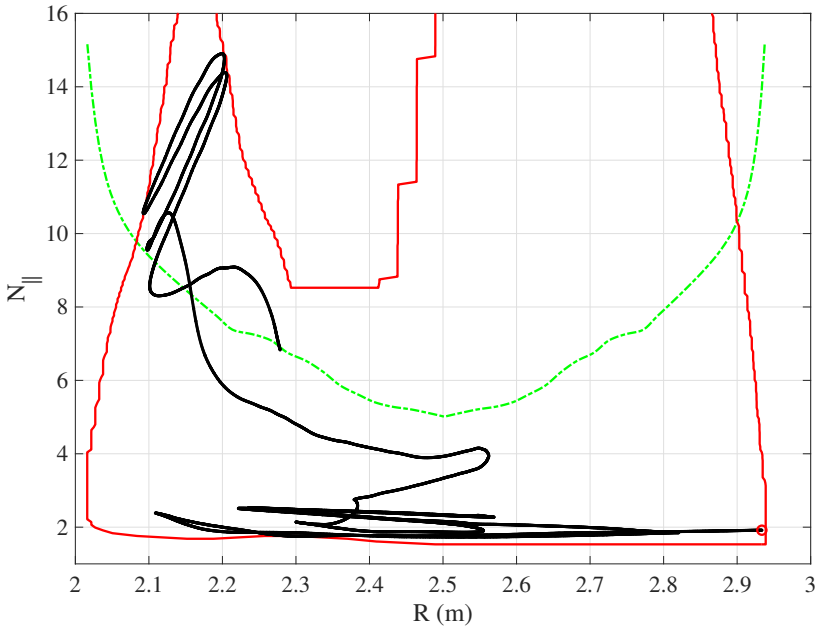

Figure 6. Red full line: propagation domain $(R, Z, N_\parallel)$ for $|N_{\parallel 0}| = 1.91$ projected on $(R, Z = Z_p, N_\parallel)$ space for the LH wave in the WEST tokamak calculated using the full electromagnetic dispersion relation. The line-averaged plasma density is $\bar{n}_e \simeq 4.6 \times 10^{+19}\, m^{-3}$, the central magnetic field is $B_{T0} = 3.57\, T$, the toroidal plasma current is $I_p = 530\, kA$, and the central safety factor is $q_0 \simeq 1.5$. Black line: corresponding ray trajectory calculated by C3PO code. The strong $N_\parallel$ upshift occurs when the ray propagates near the X-point of the magnetic configuration. The red circle highlights the ray starting point [33]. Green curve : kinetic domain of strong linear absorption for the LH wave characterized by the condition $N_\parallel = N_{\parallel L}$. The core electron temperature is $T_{e0} \simeq 1.7\, keV$. Plasma and RF wave parameters correspond to the partially driven LH discharge #55539 at $t = 9.9369\, s$ where the main lobe in the launched power spectrum calculated by ALOHA antenna coupling code is at $|N_{\parallel 0}| \simeq 1.91$ [32].

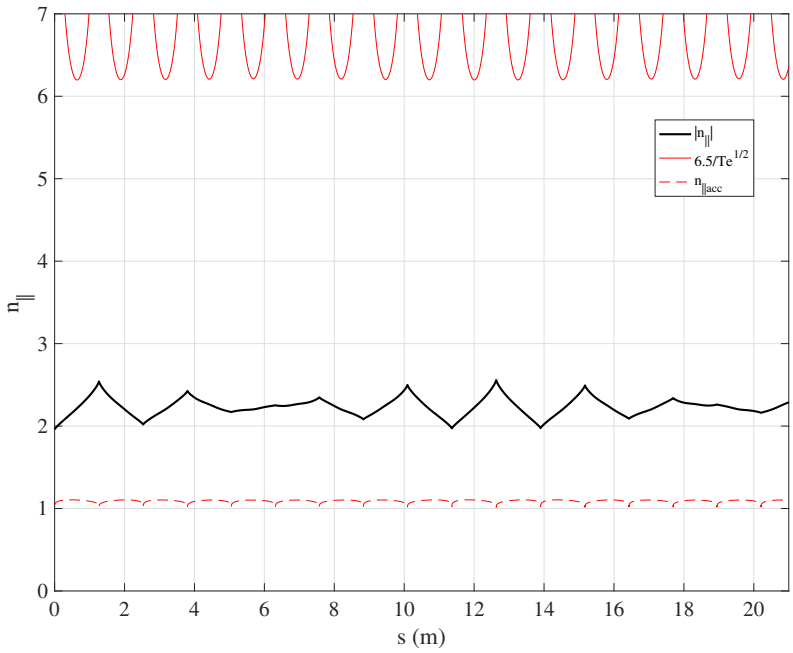

Figure 7. Black full line: $N_{\parallel}$ evolution along the ray trajectory in TRIAM-1M tokamak as function of the ray length s. Initial condition is corresponding to the main lobe launched at $\left|N_{\parallel 0}\right| = 1.96$. The variation of $N_{\parallel}$ is strongly bounded by the domain, as shown in Fig. 1; Dashed red line: $N_{\parallel acc}$ evolution along the ray trajectory; Full red line: $N_{\parallel L}$ along the ray trajectory corresponding to strong linear absorption. Since the black full line never crosses the full red line, the spectral gap is clearly unbridgeable. Calculations are performed with C3PO ray-tracing code [33].

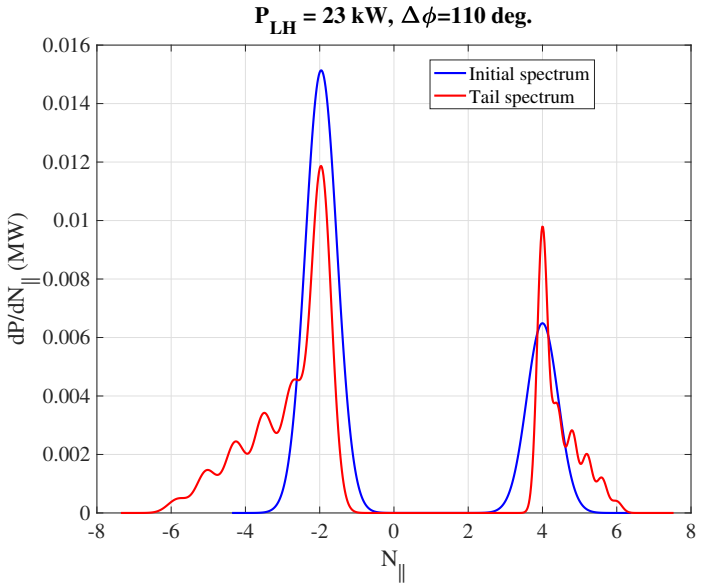

Figure 8. . Blue curve : excited power spectrum by LH antenna in TRIAM-1M tokamak, with waveguide phasing $\Delta_w = 110\,deg$ as deduced from Brambilla's grill theory [27]. Red curve : power spectrum from the tail LH model using five additional lobes up to $N_{\|L}^{\min}$,with 50% of power carried by each lobe transferred to the tail. [18, 19].

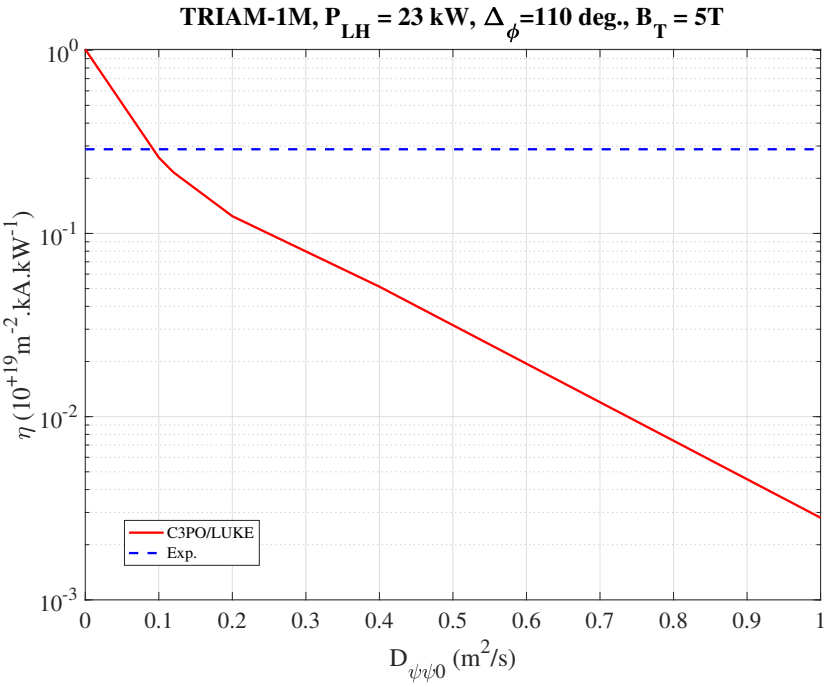

Figure 9. . Full red curve : Calculated LH current drive efficiency of the fully LH-driven discharge ($P_{LH} = 23kW$, $\Delta_w = 110\,deg.$, $B_{T0} = 5.0\,T$) as function of the anomalous radial diffusion coefficient. Blue dashed line: experimental level of the current drive efficiency in TRIAM-1M [27].

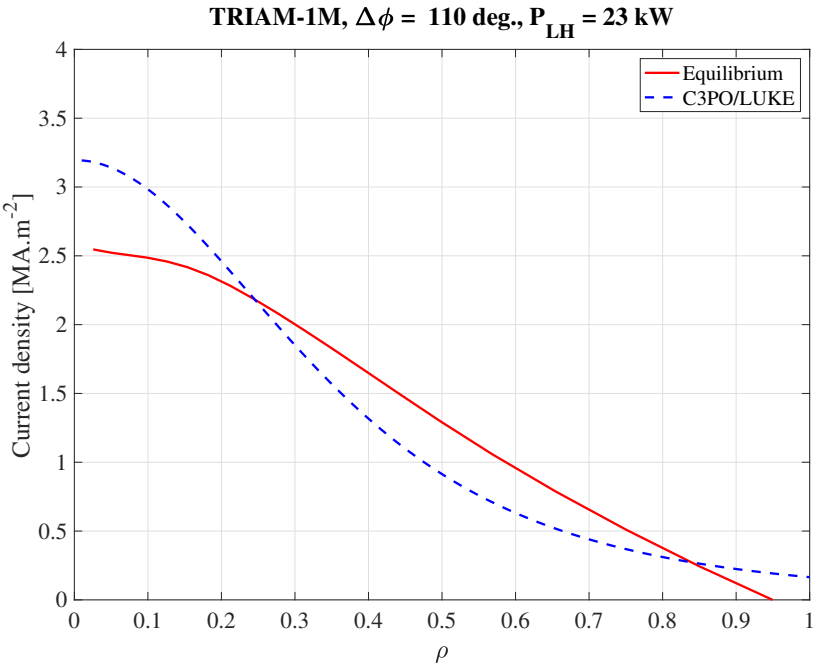

Figure 10. . Full red curve : current density profile of the toroidal MHD equilibrium for the reference TRIAM-1M LH discharge. Dashed blue curve : LH current density profile calculated by RTFP calculations. In both cases, the total plasma current is $I_p = 27.5\,kA$ corresponding to experimental observations. See main text for more details.

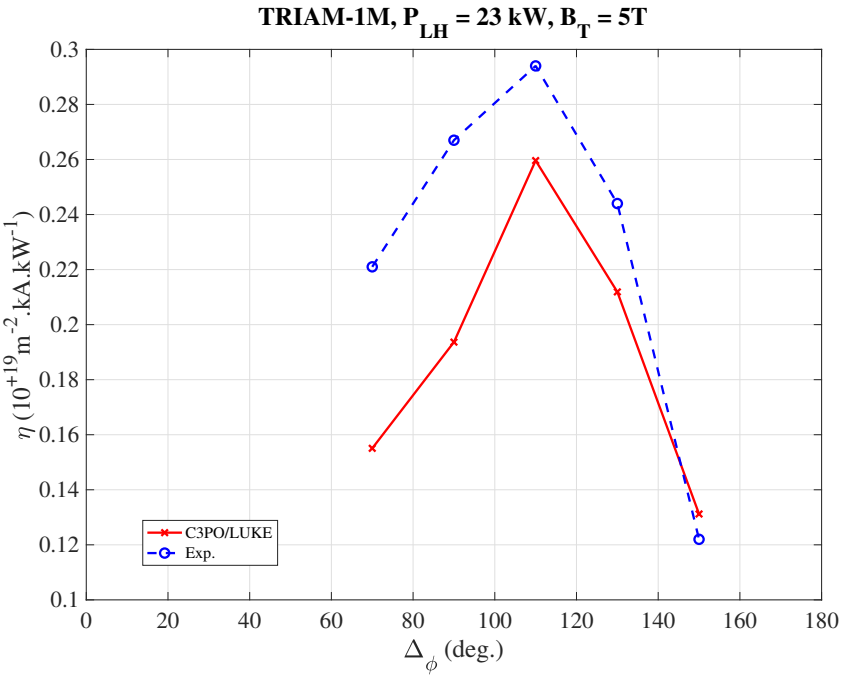

Figure 11. . Full red curve : LH current drive efficiency as calculated by RTFP for LHCD in TRIAM-1M. The maximum corresponds to $\Delta_w = 110\,deg.$ Dashed blue curve : experimental observations [27]. For all waveguide phasing, the toroidal MHD equilibrium is unchanged and corresponds to the reference case. The anomalous radial transport of the fast electrons is also unchanged.

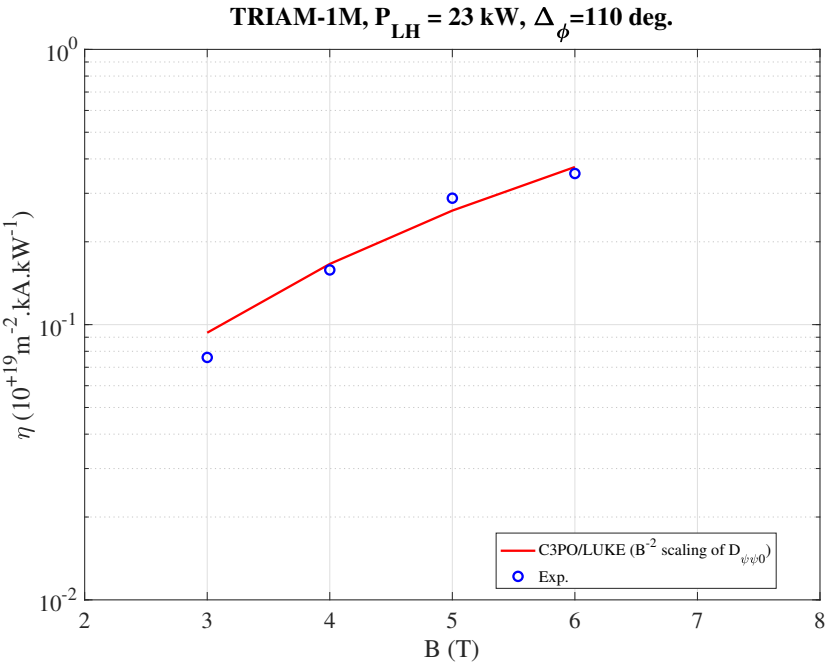

.

Figure 12. . Full red curve : variation of the LH current drive efficiency for LHCD in TRIAM-1M tokamak as function of the magnetic field toroidal magnetic B, as calculated by RTFP. In order to reproduce experimental observations (blue circle, [27]), $D_{\psi\psi 0}$ must scale like B^{-2}.

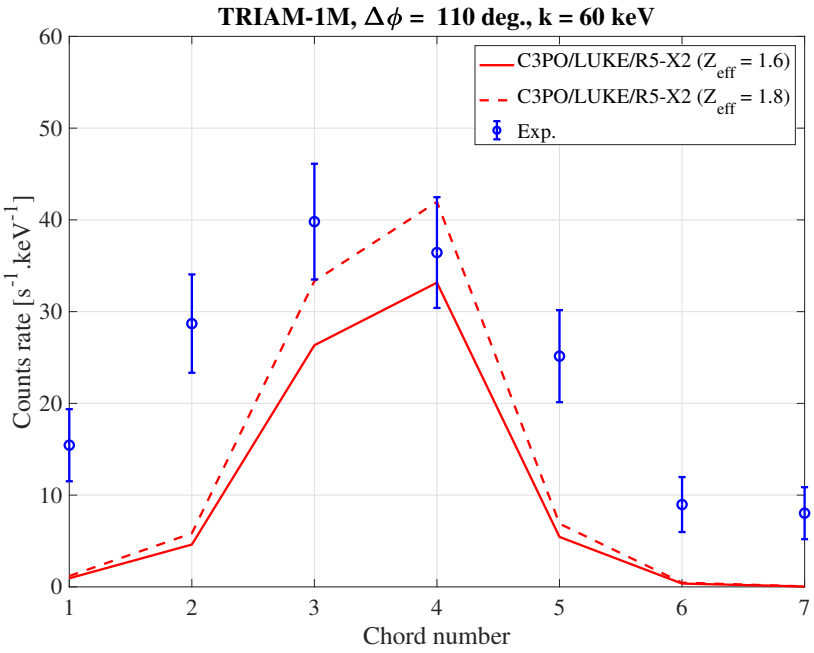

Figure 13. . Full red curve : line-integrated fast electron bremsstrahlung at photon energy $k = 60\,keV$, as calculated by RTFP and synthetic diagnostic R5-X2 for LHCD in TRIAM-1M tokamak. The effective charge is $Z_{eff} = 1.6$. Dashed red curve : same calculation, but with 15 % increase of the effective charge for the bremsstrahlung only. Blue circles : experimental observation [27]). Error bars are calculated approximately from the estimated time sampling.

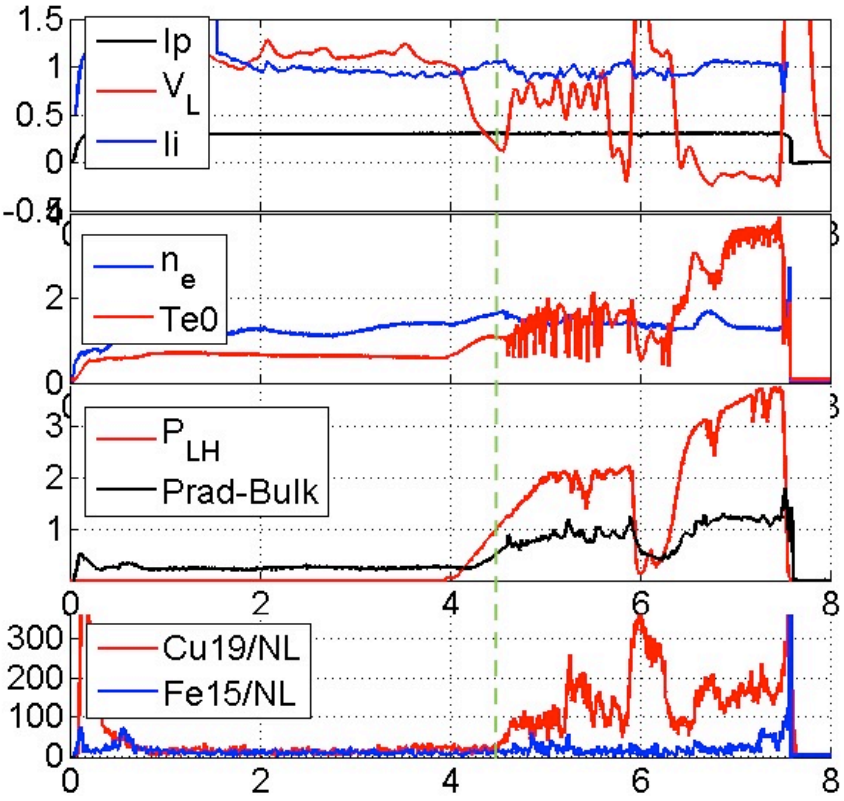

Figure 14. . Main time traces for the WEST LH-driven discharge #54952. The study is performed $t = 4.5\,s$ (green dashed line). for which full current drive is transiently achieved while high-Z impurity content remains small. At that time, LH power is coupled to the plasma using the FAM antenna.

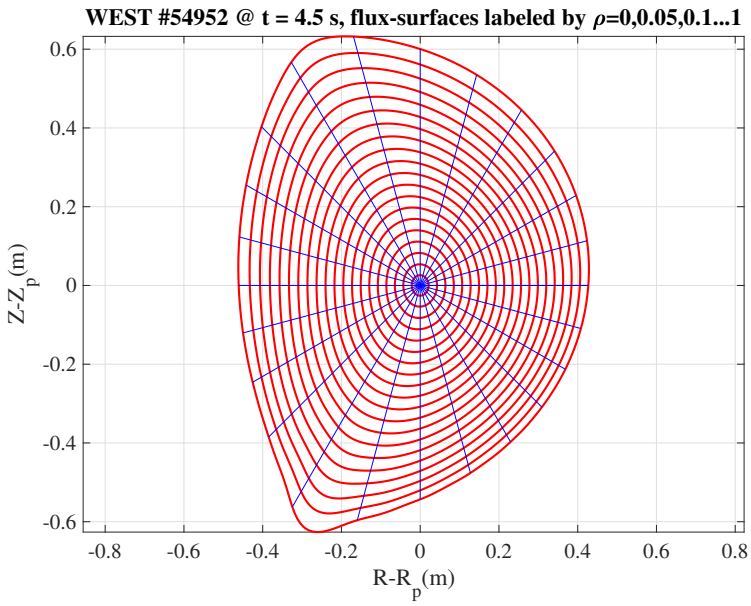

Figure 15. . Contour plot of magnetic flux surfaces labeled $\rho = 0, 0.05, 0.1...1$ for the WEST discharge #54952 at $t = 4.5\,s$, as calculated by METIS code [49]

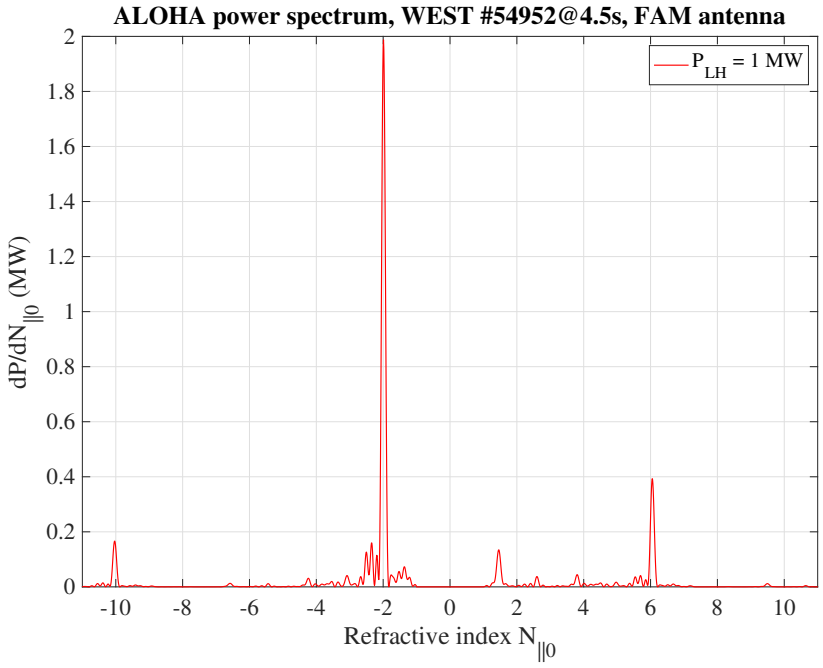

Figure 16. Power spectrum calculated by ALOHA coupling code for the WEST FAM antenna (discharge #54952 at $t = 4.5\,s$) [32]. Almost all the LH power driving the plasma current is corresponding to the main lobe at $|N_{\|0}| = 2$. Satellite lobes at $|N_{\|0}| = 6$ and $|N_{\|0}| = 10$ contribute to plasma heating but not current drive. The total launched power is $1\,MW$.

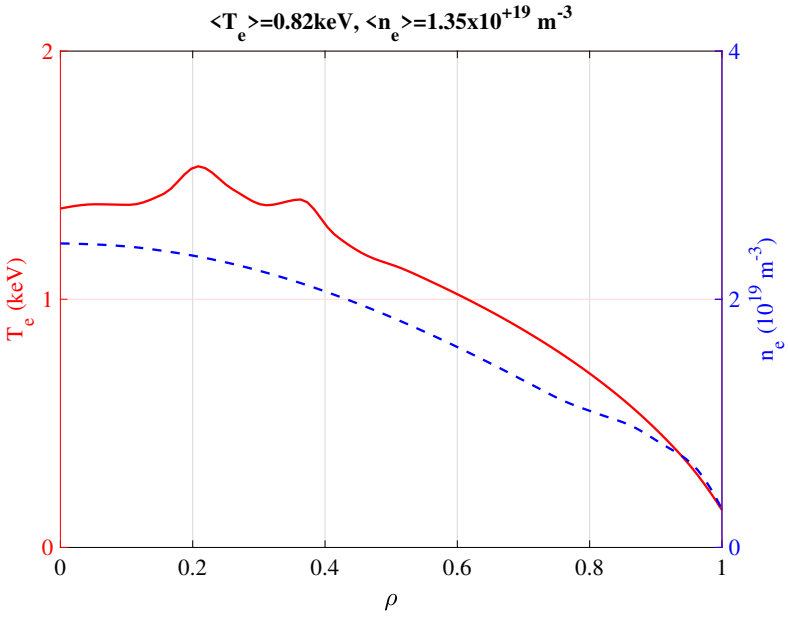

Figure 17. . Electron temperature (full red line) and density (dashed blue line) radial profiles for WEST discharge #54952 at $t = 4.5\,s$, as calculated by METIS calculations [49].

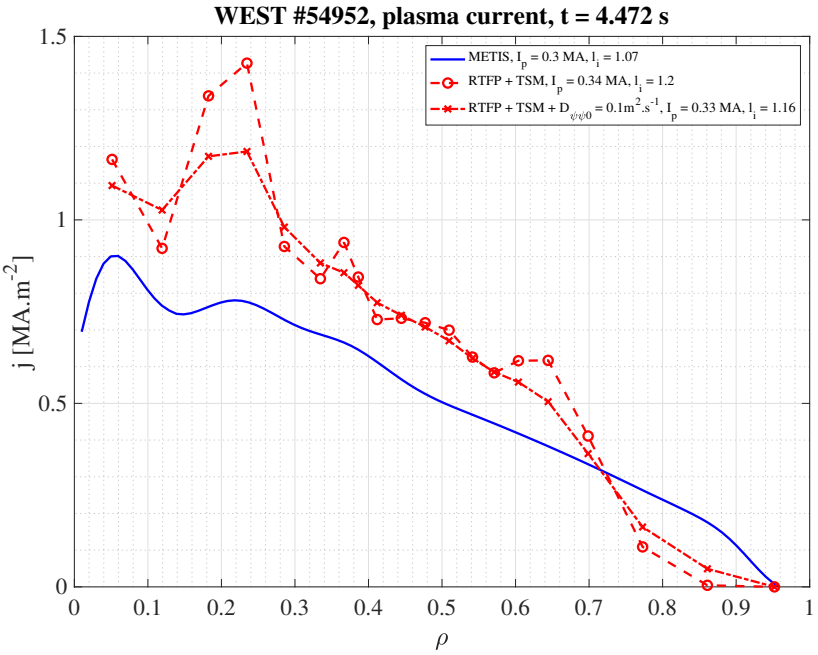

Figure 18. . Current density profile (full blue line) from METIS toroidal MHD equilibrium, and from RTFP calculations with the TSM (dashed red line and circles: $D_{\psi\psi 0} = 0.0\, m^2 s^{-1}$, dotted dashed red line and crosses: $D_{\psi\psi 0} = 0.1\, m^2 s^{-1}$) for WEST discharge #54952 at $t = 4.5\, s$. All profiles exhibit a relative maximum around $\rho = 0.2$ consistent with the small peak in the electron temperature profile (see Fig. 17).

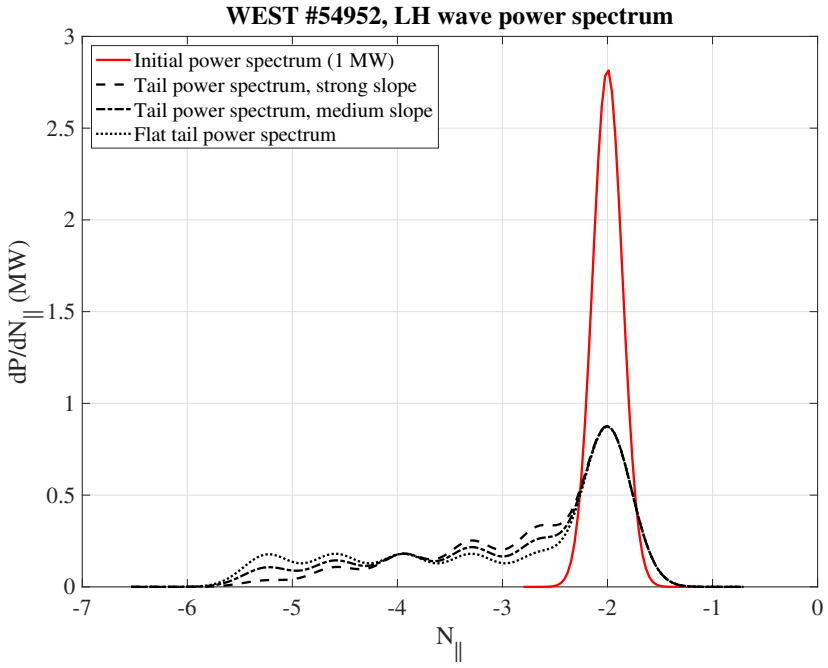

Figure 19. . Power spectra used for modeling WEST LH discharge #54952 at $t = 4.5\,s$. Red line: main Gaussian-like lobe deduced from ALOHA antenna coupling code [32]; black dotted line : flat spectral tail in $N_{\|}$; black dotted dashed line : spectral tail with a medium slope in $N_{\|}$; black dashed line : spectral tail with a strong slope in $N_{\|}$. For all spectra with a tail, 50 % of the LH power in the main lobe is transferred to the tail. For all spectra (tail and no tail), the total injected power is $P_{LH} = 1\,MW$.

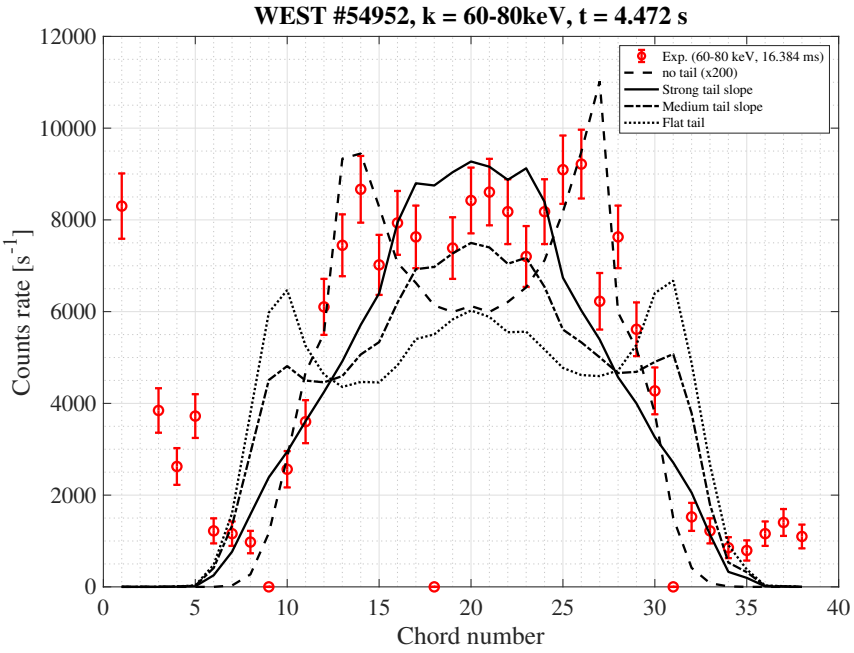

Figure 20. . Line-integrated pulse HXR profile WEST discharge #54952 at $t = 4.47\,s$ in the photon energy interval $60 - 80\,keV$. Red circle: measurements with error-bar (sampling time is 16.384 ms); blue dashed line : line-integrated fast electron bremsstrahung as calculated by RTFP and synthetic diagnostic R5-X2 with out tail. Signal is multiplied by 1000; black dotted line : C3PO/LUKE/RX-X2 calculations with flat spectral tail as shown in Fig. 19; black dotted dashed line : C3PO/LUKE/RX-X2 calculations with a spectral tail (medium slope, as shown in Fig. 19); black dashed line : C3PO/LUKE/RX-X2 calculations with a spectral tail (strong slope, as shown in Fig. 19).

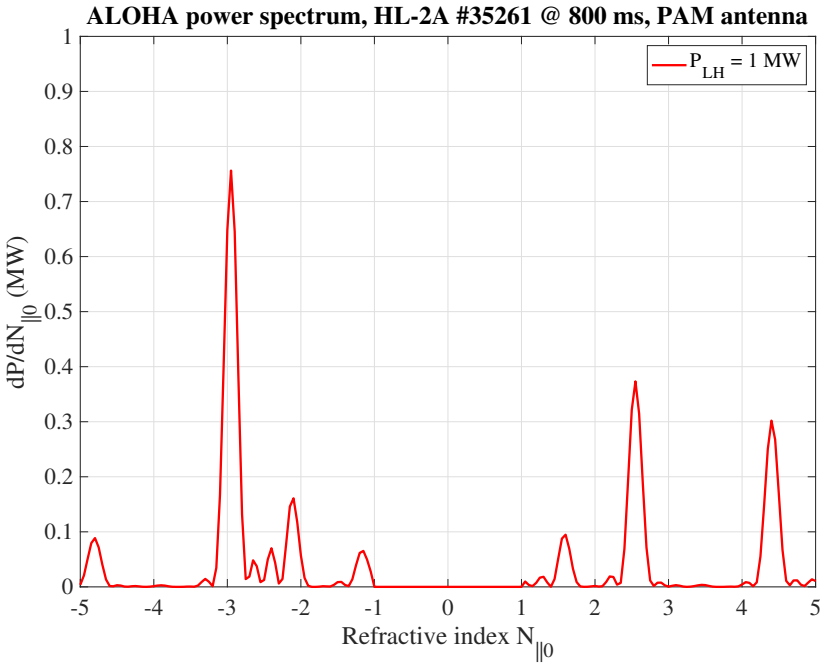

Figure 21. . Power spectrum calculated by ALOHA coupling code for the HL-2A PAM antenna (discharge #35261 at $t = 0.8\,s$) [32]. The total launched power is $840\,kW$.

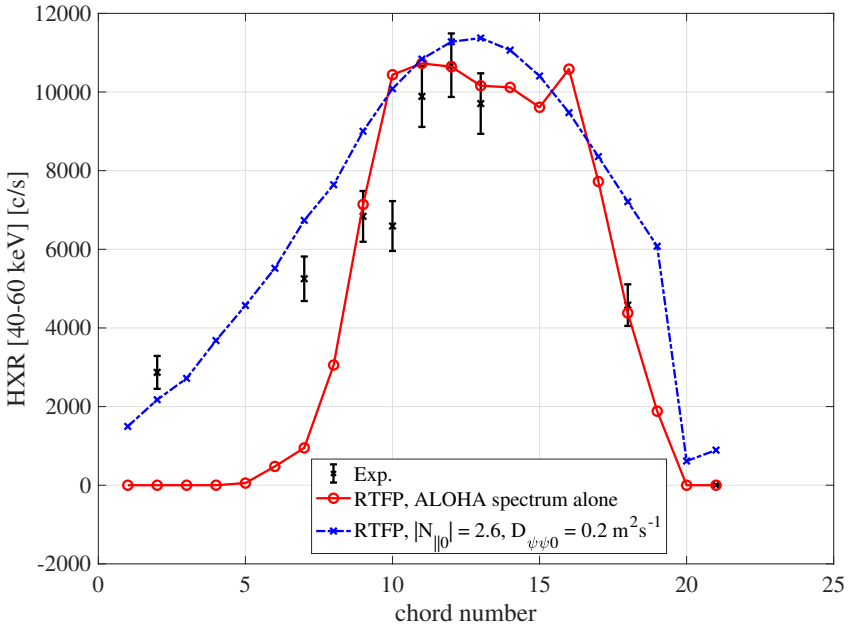

Figure 22. . Calculated (full red line and red circles : ALOHA power spectrum alone, dot dashed line and blue crosses : $\left|N_{\|0}\right| = 2.6$ and $D_{\psi\psi 0} \simeq 0.2\, m^2 s^{-1}$) and experimental (black crosses) line-integrated HXR profiles during full LH current drive. When ALOHA power spectrum is used as input, calculations are performed with the five most prominent lobes of the excited power spectrum by the PAM antenna without anomalous fast electron radial transport (HL-2A tokamak, discharge #35261 at $t = 0.8\, s$) [32]. For the case of a single lobe at $\left|N_{\|0}\right| = 2.6$, an anomalous fast electron radial transport is considered. In both cases, the total injected power is $840\, kW$. . Error bars of experimental data are calculated assuming that Poisson's statistics of photon counting holds.–

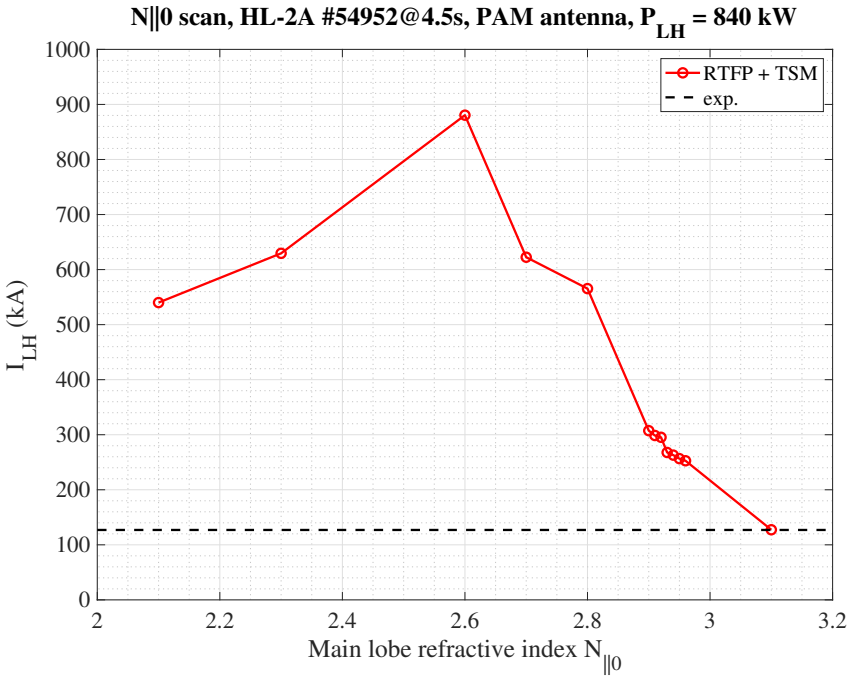

Figure 23. . Full red line and red circles : calculated LH current as function of $\left|N_{\|0}\right|$ using the TSM for the power spectrum and the experimental level (black dashed line) for the HL-2A tokamak, discharge #35261 at $t = 0.8\,s$. The total launched LH power is $840\,kW$. No anomalous fast electron radial transport.

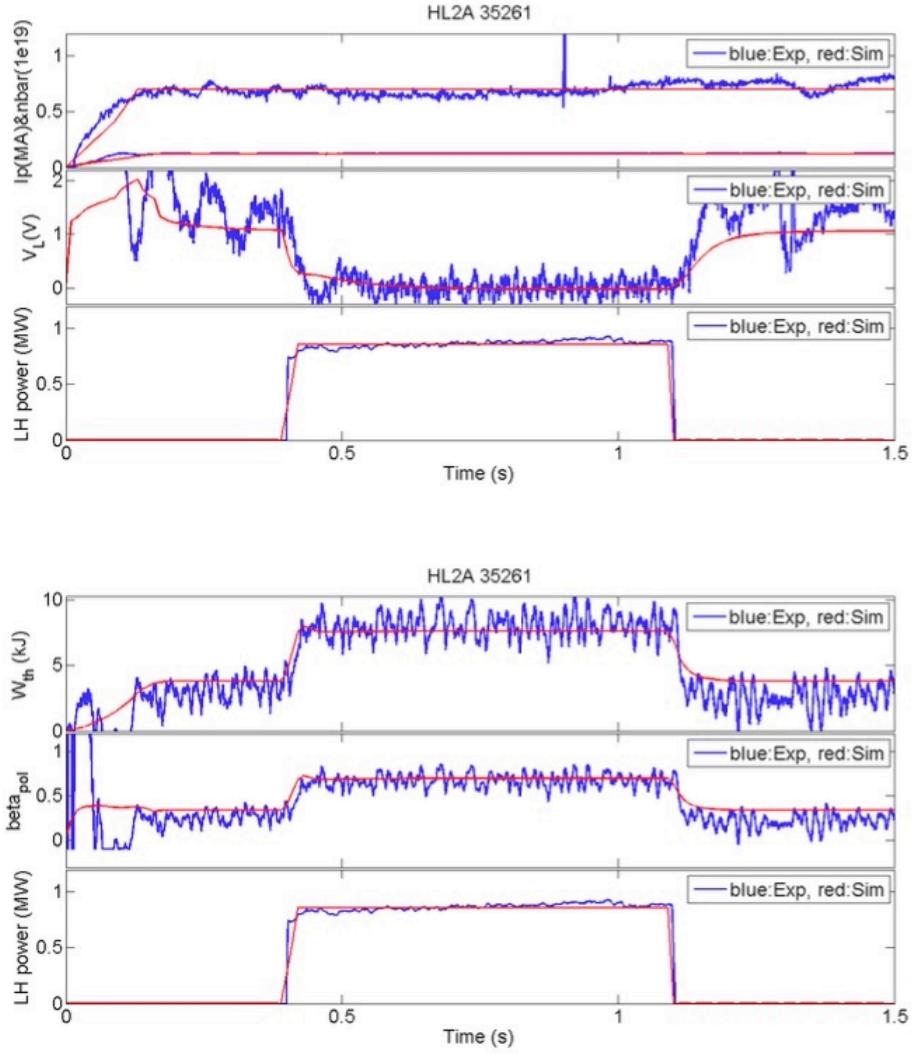

Figure 24. . Time analysis of HL-2A full current drive discharge with PAM antenna (discharge #35261) using METIS code [49]. In order to reproduce observations, power absorption must be central with a width of $\Delta\rho = 0.3$ consistent with RTFP calculations, and the current drive efficiency of $\eta \simeq 0.18 \times 10^{+19}(AW^{-1}m^{-2})$.